Journal of Computational Physics 245 (2013) 131–149

Contents lists available at SciVerse ScienceDirect

Journal of Computational Physics

journal homepage: www.elsevier.com/locate/jcp

Numerical methods for nonlinear Dirac equation

Jian Xu [a], Sihong Shao [a,*], Huazhong Tang [b]

[a] LMAM and School of Mathematical Sciences, Peking University, Beijing 100871, China
[b] HEDPS, CAPT & LMAM, School of Mathematical Sciences, Peking University, Beijing 100871, China

ARTICLE INFO

Article history:
Received 23 December 2012
Received in revised form 4 March 2013
Accepted 11 March 2013
Available online 27 March 2013

Keywords:
Nonlinear Dirac equation
Solitary wave
Interaction dynamics
Finite difference method
Operator splitting method

ABSTRACT

This paper presents a review of the current state-of-the-art of numerical methods for nonlinear Dirac (NLD) equation. Several methods are extendedly proposed for the (1 + 1)-dimensional NLD equation with the scalar and vector self-interaction and analyzed in the way of the accuracy and the time reversibility as well as the conservation of the discrete charge, energy and linear momentum. Those methods are the Crank–Nicolson (CN) schemes, the linearized CN schemes, the odd–even hopscotch scheme, the leapfrog scheme, a semi-implicit finite difference scheme, and the exponential operator splitting (OS) schemes. The nonlinear subproblems resulted from the OS schemes are analytically solved by fully exploiting the local conservation laws of the NLD equation. The effectiveness of the various numerical methods, with special focus on the error growth and the computational cost, is illustrated on two numerical experiments, compared to two high-order accurate Runge–Kutta discontinuous Galerkin methods. Theoretical and numerical comparisons show that the high-order accurate OS schemes may compete well with other numerical schemes discussed here in terms of the accuracy and the efficiency. A fourth-order accurate OS scheme is further applied to investigating the interaction dynamics of the NLD solitary waves under the scalar and vector self-interaction. The results show that the interaction dynamics of two NLD solitary waves depend on the exponent power of the self-interaction in the NLD equation; collapse happens after collision of two equal one-humped NLD solitary waves under the cubic vector self-interaction in contrast to no collapse scattering for corresponding quadric case.

1. Introduction

As a relativistic wave equation, the Dirac equation provides naturally a description of an electron [1]. Following Dirac's discovery of the linear equation of the electron, there appears the fundamental idea of nonlinear description of an elementary spin-1/2 particle which makes it possible to take into account its self-interaction [2–4]. Heisenberg put forward the idea to use a nonlinear Dirac (NLD) equation as a possible basis model for a unified field theory [5]. A key feature of the NLD equation is that it allows solitary wave solutions or particle-like solutions — the stable localized solutions with finite energy and charge [6]. That is, the particles appear as intense localized regions of field which can be recognized as the basic ingredient in the description of extended objects in quantum field theory [7]. Different self-interactions give rise to different NLD models mainly including the Thirring model [8], the Soler model [9], the Gross–Neveu model [10] (equivalent to the massless Soler model), and the bag model [11] (*i.e.* the solitary waves with finite compact support), all of which attracted wide interest of

* Corresponding author. Tel.: +86 1062751801.
E-mail addresses: xujian764@gmail.com (J. Xu), sihong@math.pku.edu.cn (S. Shao), hztang@math.pku.edu.cn (H. Tang).

0021-9991/$ - see front matter © 2013 Elsevier Inc. All rights reserved.
http://dx.doi.org/10.1016/j.jcp.2013.03.031

physicists and mathematicians around the 1970s and 1980s, especially on looking for the solitary wave solutions and investigating the related physical and mathematical properties [6].

For the NLD equation in (1 + 1) dimensions (*i.e.* one time dimension plus one space dimension), several analytical solitary wave solutions are derived in [12,13] for the quadric nonlinearity, [14] for fractional nonlinearity as well as [15,16] for general nonlinearity by using explicitly the constraint resulting from energy-momentum conservation, and summarized by Mathieu [17]. In contrast, there are few explicit solutions in (1 + 3) dimensions except for some particular cases shown in [18] in spite of their existence claimed by mathematicians for various situations [19–26] (the readers are referred to an overview [27] on this topic), and most understanding is based on numerical investigations, *e.g.* [28–30]. Beyond this, the study of the NLD equation in (1 + 1) dimensions could be very helpful for that in (1 + 3) dimensions since the (1 + 1)-dimensional NLD equation correspond to the asymptotic form of the equation in the physically interesting case of (1 + 3) dimensions as emphasized by Kaus [31]. That is, some qualitative properties of the NLD solitary waves could be similar in such two cases. An interesting topic for the NLD equation is the stability issue, which has been the central topic in works spread out over several decades in an effort that is still ongoing. Analytical studies of the NLD solitary wave stability face serious obstacles [32–34], while results of computer simulations are contradictory [35–37,30]. The stability analysis of the NLD solitary waves is still a very challenging mathematical problem to date [38,16]. Recent efforts in this direction can be found in [39–44]. Another rising mathematical interest related to the NLD equation is the analysis of global well-posedness, *e.g.* see [45,46] and references therein.

In the case of that theoretical methods were not able to give the satisfactory results, numerical methods were used for obtaining the solitary wave solutions of the NLD equation as well as for investigating the stability. An important step in this direction was made by Alvarez and Carreras [47], who simulated the interaction dynamics between the (1 + 1)-dimensional NLD solitary waves of different initial charge for the Soler model [9] by using a second-order accurate Crank–Nicholson (CN) scheme [48]. They first saw there: charge and energy interchange except for some particular initial velocities of the solitary waves; inelastic interaction in binary collisions; and oscillating state production from binary collisions. Motivated by their work, Shao and Tang revisited this interaction dynamics problem in 2005 [49] by employing a fourth-order accurate Runge–Kutta discontinuous Galerkin (RKDG) method [50]. They not only recovered the phenomena mentioned by Alvarez and Carreras but also revealed several new ones, *e.g.* collapse in binary and ternary collisions of two-humped NLD solitary waves [49]; a long-lived oscillating state formed with an approximate constant frequency in collisions of two standing waves [50]; full repulsion in binary and ternary collisions of out-of-phase waves [51]. Their numerical results also inferred that the two-humped profile could undermine the stability during the scattering of the NLD solitary waves. Note in passing that the two-humped profile was first pointed out by Shao and Tang [49] and later gotten noticed by other researchers [16]. Besides the often-used CN [48] and RKDG methods [50], there exist many other numerical schemes for solving the (1 + 1)-dimensional NLD equation: split-step spectral schemes [52], the linearized CN scheme [53], the semi-implicit scheme [54]46, Legendre rational spectral methods [55], multi-symplectic Runge–Kutta methods [56], adaptive mesh methods [57] *etc*. The fourth-order accurate RKDG method [50] is very appropriate for investigating the interaction dynamics of the NLD solitary waves due to their ability to capture the discontinuous or strong gradients without producing spurious oscillations, and thus performs better than the second-order accurate CN scheme [48]. However, the high cost due to the relatively more freedoms used in each cell and the stringent time step constraint reduce its practicality in more realistic simulations where realtime and quantitative results are required.

Recently, there has been a remarkable upsurge of the interest in the NLD models, as they emerge naturally as practical models in other physical systems, such as the gap solitons in nonlinear optics [38], Bose–Einstein condensates in honeycomb optical lattices [58], as well as matter influencing the evolution of the Universe in cosmology [59]. In view of such new trend, longtime stable, efficient, conservative and high-order accurate numerical methods for solving the NLD equation are highly desirable. Finite difference methods, usually as the first try in practice, enable easy coding and debugging and thus are often used by physicists and engineers. However, detailed discussion and careful comparison on finite difference solvers for the NLD equation are not existed. To this end, the present work as the first step will extendedly propose the finite deference schemes for solving the NLD equation with the scalar and vector self-interaction. A general and precise comparison among them will be presented. However, all of these finite difference methods are often of the second order accuracy and thus sustain fast error growth with respect to time. To achieve relatively slow error growth, high-order accurate numerical methods are required. By exploiting the local conservation laws of the NLD equation, we present exponential operator splitting (OS) schemes which are time reversible and can conserve the discrete charge. One of the high-order accurate OS schemes is afterwards adopted to investigate the interaction dynamics for the NLD solitary waves under the general scalar and vector self-interaction. It should be noted that the experiments carried out in the literatures are all limited to the collisions of the NLD solitary waves under the quadric scalar self-interaction. Here, the binary collisions of the NLD solitary waves under the cubic scalar self-interaction or under the vector self-interaction or under the linear combination of the scalar and vector self-interactions are all studied for the first time.

The paper is organized as follows. There is a brief review of the NLD equation in Section 2 and the solitary wave solutions are also derived there for the general scalar and vector self-interaction. The numerical schemes are presented in Section 3 and corresponding numerical analysis is given in Section 4. The numerical results are presented with discussion in Section 4. The paper is concluded in Section 6 with a few remarks.

2. Preliminaries and notations

This section will introduce the (1 + 1)-dimensional NLD equation with the scalar and vector self-interaction and derive its two solitary wave solutions. Throughout the paper, units in which both the speed of light and the reduced Planck constant are equal to one will be used.

2.1. Nonlinear Dirac equation

Our attention is restricted to the NLD equation in $(1+1)$ dimensions which can be written in the covariant form

$$(\mathrm{i}\boldsymbol{\gamma}^{\mu}\partial_{\mu} - m)\boldsymbol{\Psi} + \partial L_{\mathrm{l}}[\boldsymbol{\Psi}]/\partial\bar{\boldsymbol{\Psi}} = 0, \tag{2.1}$$

where $\boldsymbol{\Psi}$ is the spinor with two complex components, $\bar{\boldsymbol{\Psi}} := \boldsymbol{\Psi}^{\dagger}\boldsymbol{\gamma}^{0}$ denotes the adjoint spinor, $\boldsymbol{\Psi}^{\dagger}$ is the complex conjugate transpose of $\boldsymbol{\Psi}$, $L_{\mathrm{l}}[\boldsymbol{\Psi}]$ denotes the self-interaction Lagrangian, the Greek index μ runs from 0 to 1, the Einstein summation convection has been applied, i is the imaginary unit, m is the rest mass, $\partial_{\mu} = \frac{\partial}{\partial x^{\mu}}$ stands for the covariant derivative, and $\boldsymbol{\gamma}^{\mu}$, for $\mu = 0, 1$, are the gamma matrices or the Dirac matrices, chosen as those in [47,49],

$$\boldsymbol{\gamma}^{0} = \begin{pmatrix} 1 & 0 \\ 0 & -1 \end{pmatrix}, \quad \boldsymbol{\gamma}^{1} = \begin{pmatrix} 0 & 1 \\ -1 & 0 \end{pmatrix}.$$

In fact, Eq. (2.1) is the equation of motion for the classical spinorial particle with the Lagrangian being a sum of the Dirac Lagrangian and the self-interaction Lagrangian, *i.e.*

$$L[\boldsymbol{\Psi}] = \bar{\boldsymbol{\Psi}}(\mathrm{i}\boldsymbol{\gamma}^{\mu}\partial_{\mu} - m)\boldsymbol{\Psi} + L_{\mathrm{l}}[\boldsymbol{\Psi}]. \tag{2.2}$$

There exist several different NLD models in the literature, where two important models in (1 + 1) dimensions are the scalar self-interaction of Soler [9]

$$L_{\mathrm{s}}[\boldsymbol{\Psi}] := \bar{\boldsymbol{\Psi}}\boldsymbol{\Psi} \tag{2.3}$$

and the vector self-interaction of Thirring [60]

$$L_{\mathrm{v}}[\boldsymbol{\Psi}] := \bar{\boldsymbol{\Psi}}\boldsymbol{\gamma}^{\mu}\boldsymbol{\Psi}\bar{\boldsymbol{\Psi}}\boldsymbol{\gamma}_{\mu}\boldsymbol{\Psi}, \tag{2.4}$$

where $\boldsymbol{\gamma}_{\mu} = \eta_{\mu\nu}\boldsymbol{\gamma}^{\nu}$ with the Minkowski metric $\eta_{\mu\nu} = \mathrm{diag}(1, -1)$ on spacetime, which implies $\boldsymbol{\gamma}_{\mu} = (-1)^{\mu}\boldsymbol{\gamma}^{\mu}$.

This paper will focus on the NLD Eq. (2.1) with a more general self-interaction [15,61]

$$L_{\mathrm{l}}[\boldsymbol{\Psi}] = s(L_{\mathrm{s}}[\boldsymbol{\Psi}])^{k+1} + v(L_{\mathrm{v}}[\boldsymbol{\Psi}])^{(k+1)/2} \tag{2.5}$$

and extendedly propose and compare its numerical methods, where s and v are two real numbers and k is a positive real number. If the spinor $\boldsymbol{\Psi}$ is scaled by a constant factor as $\boldsymbol{\Psi}' = \sqrt{\alpha}\boldsymbol{\Psi}$ with $\alpha \in \mathbb{C}$, then the scaled self-interaction Lagrangian will be $\alpha^{k+1}L_{\mathrm{l}}[\boldsymbol{\Psi}]$ which shows that the power exponent to α is $k+1$. In such sense, we call that the self-interaction Lagrangian L_{l} has the power exponent $k+1$ [14–16]. Hereafter the *quadric* and *cubic* self-interaction will be referred to the case $k = 1$ and the case $k = 2$, respectively.

The self-interaction (2.5) implies the so-called homogeneity relation [17,15]

$$\bar{\boldsymbol{\Psi}}\frac{\partial L_{\mathrm{l}}[\boldsymbol{\Psi}]}{\partial\bar{\boldsymbol{\Psi}}} = (k+1)L_{\mathrm{l}}[\boldsymbol{\Psi}].$$

Combining it with the definition of the Lagrangian $L[\boldsymbol{\Psi}]$ and (2.1) gives

$$L[\boldsymbol{\Psi}] = -kL_{\mathrm{l}}[\boldsymbol{\Psi}]. \tag{2.6}$$

¶For the NLD Eq. (2.1) with (2.5), one may still verify the following local conservation laws for the current vector J_{μ} and the energy-momentum tensor $T_{\mu\nu}$:

$$\partial^{\mu}J_{\mu} = 0, \quad \partial^{\mu}T_{\mu\nu} = 0, \tag{2.7}$$

where

$$J_{\mu} = \bar{\boldsymbol{\Psi}}\boldsymbol{\gamma}_{\mu}\boldsymbol{\Psi}, \quad T_{\mu\nu} = \mathrm{i}\bar{\boldsymbol{\Psi}}\boldsymbol{\gamma}_{\mu}\partial_{\nu}\boldsymbol{\Psi} - \eta_{\mu\nu}L[\boldsymbol{\Psi}].$$

For localized solitary waves $\boldsymbol{\Psi} = (\psi_1, \psi_2)^T$, one may derive a direct corollary of (2.7), *i.e.* the following global conservation laws [50].

Proposition 2.1. *Assume that* $\lim_{|x|\to+\infty}|\psi_i(x,t)| = 0$ *and* $\lim_{|x|\to+\infty}|\partial_x\psi_i(x,t)| < +\infty$ *hold uniformly for* $t \geqslant 0$ *and* $i = 1, 2$. *The total energy E, the total linear momentum P, and the total charge Q, defined respectively by*

$$E(t) := \int_{-\infty}^{+\infty} T_{00}\mathrm{d}x, \quad P(t) := \int_{-\infty}^{+\infty} T_{01}\mathrm{d}x, \quad Q(t) := \int_{-\infty}^{+\infty} J_0\mathrm{d}x, \tag{2.8}$$

satisfy

$$\frac{\mathrm{d}}{\mathrm{d}t}E(t)=0,\quad \frac{\mathrm{d}}{\mathrm{d}t}P(t)=0,\quad \frac{\mathrm{d}}{\mathrm{d}t}Q(t)=0.$$

The properties (2.6) and (2.7) will be also exploited to find the solitary wave solutions of the (1 + 1)-dimensional NLD Eq. (2.1) with L_{I} given in (2.5) in the next subsection.

2.2. Standing wave solution

This subsection will derive the standing wave solutions of the (1 + 1)-dimensional NLD Eq. (2.1) with the self-interaction (2.5) in the spirit of the technique used in [12,13,17,15]. The solution $\boldsymbol{\Psi}=(\psi_1,\psi_2)^T$ of the NLD Eq. (2.1) with L_{I} in (2.5), having the form

$$\psi_1(x,t)=\mathrm{e}^{-\mathrm{i}\omega t}\varphi(x),\quad \psi_2(x,t)=\mathrm{e}^{-\mathrm{i}\omega t}\chi(x)$$

is wanted, where $m>\omega\geqslant 0$, and $|\varphi(x)|$ and $|\chi(x)|$ are assumed to decay exponentially as $|x|\to+\infty$ or have the finite compact support. For such solution, it is not difficult to verify that both the Lagrangian $L[\boldsymbol{\Psi}]$ and the energy-momentum tensor $T_{\mu\nu}$ are independent of the time t, because

$$\begin{aligned}&L[\boldsymbol{\Psi}]\equiv\omega\bar{\boldsymbol{\psi}}\boldsymbol{\gamma}^0\boldsymbol{\psi}+\mathrm{i}\bar{\boldsymbol{\psi}}\boldsymbol{\gamma}^1\boldsymbol{\psi}_x-m\bar{\boldsymbol{\psi}}\boldsymbol{\psi}+L_{\mathrm{I}}[\boldsymbol{\Psi}],\\&T_{00}\equiv-\mathrm{i}\bar{\boldsymbol{\psi}}\boldsymbol{\gamma}^1\boldsymbol{\psi}_x+m\bar{\boldsymbol{\psi}}\boldsymbol{\psi}-L_{\mathrm{I}}[\boldsymbol{\Psi}],\quad T_{01}\equiv\mathrm{i}\bar{\boldsymbol{\psi}}\boldsymbol{\gamma}^0\boldsymbol{\psi}_x,\\&T_{10}\equiv-\omega\bar{\boldsymbol{\psi}}\boldsymbol{\gamma}^1\boldsymbol{\psi},\quad T_{11}\equiv-\mathrm{i}\bar{\boldsymbol{\psi}}\boldsymbol{\gamma}^1\boldsymbol{\psi}_x+L[\boldsymbol{\Psi}],\end{aligned}\tag{2.9}$$

where $\boldsymbol{\psi}(x)=(\varphi(x),\chi(x))^T$. Using the conservation laws (2.7) further gives

$$T_{10}=-\omega\bar{\boldsymbol{\psi}}\boldsymbol{\gamma}^1\boldsymbol{\psi}=0,\quad T_{11}=-\mathrm{i}\bar{\boldsymbol{\psi}}\boldsymbol{\gamma}^1\boldsymbol{\psi}_x+L[\boldsymbol{\Psi}]=0.\tag{2.10}$$

The first equation implies that $\varphi^*\chi$ is imaginary because

$$\bar{\boldsymbol{\psi}}\boldsymbol{\gamma}^1\boldsymbol{\psi}=\varphi^*\chi+\varphi\chi^*=0.$$

Thus, without loss of generality, we may assume that $\varphi(x)$ is real and $\chi(x)$ is imaginary, and they are in the form

$$\boldsymbol{\psi}(x)=\begin{pmatrix}\varphi(x)\\ \chi(x)\end{pmatrix}=R(x)\begin{pmatrix}\cos(\theta(x))\\ \mathrm{i}\sin(\theta(x))\end{pmatrix},\tag{2.11}$$

where both $R(x)$ and $\theta(x)$ are pending real functions, and $R(x)$ is assumed to satisfy the inequality $Q(t)\equiv\int_{-\infty}^{+\infty}R^2(x)\mathrm{d}x<+\infty$. On the other hand, combining the first equation in (2.9) with the second equation in (2.10) yields

$$\omega\boldsymbol{\psi}^\dagger\boldsymbol{\psi}-m\bar{\boldsymbol{\psi}}\boldsymbol{\psi}+L_{\mathrm{I}}[\boldsymbol{\Psi}]=0,\tag{2.12}$$

which becomes for (2.11)

$$R^2(\omega-m\cos(2\theta))+R^{2k+2}(s\cos^{k+1}(2\theta)+v)=0.\tag{2.13}$$

Combining (2.12) with (2.6) leads to

$$k\omega\boldsymbol{\psi}^\dagger\boldsymbol{\psi}-km\bar{\boldsymbol{\psi}}\boldsymbol{\psi}-\mathrm{i}\bar{\boldsymbol{\psi}}\boldsymbol{\gamma}^1\boldsymbol{\psi}_x=0,$$

which reduces to for (2.11)

$$\frac{\mathrm{d}\theta}{\mathrm{d}x}=-k(\omega-m\cos(2\theta)).\tag{2.14}$$

Because

$$\int_0^\theta\frac{\mathrm{d}\tilde{\theta}}{-k\omega+km\cos(2\tilde{\theta})}=\frac{1}{\sqrt{k^2(m^2-\omega^2)}}\tanh^{-1}\left(\frac{k(m+\omega)}{\sqrt{k^2(m^2-\omega^2)}}\tan(\theta)\right)$$

for $\theta\in(-0.5\cos^{-1}(\omega/m),0.5\cos^{-1}(\omega/m))\subset(-\pi/2,\pi/2)$ when $m>\omega\geqslant 0$, the solution of (2.14) may be derived as follows:

$$\theta(x)=\tan^{-1}\left(\sqrt{\frac{m-\omega}{m+\omega}}\tanh\left(k\sqrt{m^2-\omega^2}x\right)\right)\tag{2.15}$$

for initial data $\theta(0)=0$ and $k>0$. In fact, under the previous assumption, one may verify $\theta(x)\in(-\pi/4,\pi/4)$. If coefficients s and v in (2.5) belong to the set $\{v\geqslant 0,s>-v\}$ for $m>\omega>0$, or $\{v>0,s>-v\}$ for $m>\omega=0$, then from Eq. (2.13) one has non-trivial $R(x)$ for the localized solution as follows

$$R(x)=\pm\left(\frac{m\cos(2\theta(x))-\omega}{s\cos^{k+1}(2\theta(x))+\nu}\right)^{1/2k}. \tag{2.16}$$

Hereto, the standing wave solution of the NLD Eq. (2.1) with (2.5) has been derived, and will be denoted as follows

$$\boldsymbol{\Psi}^{\mathrm{sw}}(x,t)=\begin{pmatrix}\psi_1^{\mathrm{sw}}(x,t)\\ \psi_2^{\mathrm{sw}}(x,t)\end{pmatrix}=\mathrm{e}^{-\mathrm{i}\omega t}R(x)\begin{pmatrix}\cos(\theta(x))\\ \mathrm{i}\sin(\theta(x))\end{pmatrix}, \tag{2.17}$$

where $\theta(x)$ and $R(x)$ are given in Eqs. (2.15) and (2.16), respectively. This solution represents a solitary wave with zero velocity and contains some special cases in the literature *e.g.* [47,16].

Remark 2.1. It has been pointed out in [49] that the profile of the charge density $J_0(x,t)$ for the standing wave (2.17) under the scalar self-interaction (*i.e.* $s\neq 0$ and $\nu=0$) with $k=1$ can be either one-humped or two-humped, which is also recently confirmed for any $k>0$ by other researchers in [16]. They further pointed out there that the profile can only be one-humped for any $k>0$ in the case of $s=0$ and $\nu\neq 0$. For the linear combined self-interaction (2.5) with $s\neq 0$ and $\nu\neq 0$, we find that the profile can also be one-humped (see Figs. 2 and 6 where the charge density is denoted by $\rho_{\mathrm{Q}}(x,t)$ for convenience) or two-humped (see Fig. 8).

2.3. Solitary wave solution with nonzero velocity

This subsection will derive another solution of the (1 + 1)-dimensional NLD Eq. (2.1) with the self-interaction (2.5) by using the Lorentz covariance of the NLD equation. Consider a frame F with an observer O and coordinates (x,t). The observer O describes a particle by the wavefunction $\boldsymbol{\Psi}(x,t)$ which obeys the NLD Eq. (2.1) with L_{I} given in (2.5), *i.e.*

$$\left(\mathrm{i}\boldsymbol{\gamma}^0\frac{\partial}{\partial t}+\mathrm{i}\boldsymbol{\gamma}^1\frac{\partial}{\partial x}-m\right)\boldsymbol{\Psi}(x,t)+\left(\partial L_{\mathrm{I}}[\boldsymbol{\Psi}]/\partial\bar{\boldsymbol{\Psi}}\right)(x,t)=0. \tag{2.18}$$

In another inertial frame F′ with an observer O′ and coordinates (x',t') given by the Lorentz transformation with a translation in the x-direction

$$x'=\gamma((x-x_0)-Vt),\quad t'=\gamma(t-V(x-x_0)), \tag{2.19}$$

which is called "boost" in the x-direction, where x_0 is any given position, V is the relative velocity between frames in the x-direction, and $\gamma=1/\sqrt{1-V^2}$ is the Lorentz factor. According to the relativity principle, the observer O′ describes the same particle by $\boldsymbol{\Psi}'(x',t')$ which should also satisfy

$$\left(\mathrm{i}\boldsymbol{\gamma}^0\frac{\partial}{\partial t'}+\mathrm{i}\boldsymbol{\gamma}^1\frac{\partial}{\partial x'}-m\right)\boldsymbol{\Psi}'(x',t')+\left(\partial L_{\mathrm{I}}'[\boldsymbol{\Psi}']/\partial\bar{\boldsymbol{\Psi}}'\right)(x',t')=0. \tag{2.20}$$

Using some algebraic manipulations, the "transformation" matrix $\boldsymbol{S}$ may be found as follows

$$\boldsymbol{S}=\begin{pmatrix}\sqrt{\frac{\gamma+1}{2}} & \mathrm{sign}(V)\sqrt{\frac{\gamma-1}{2}}\\ \mathrm{sign}(V)\sqrt{\frac{\gamma-1}{2}} & \sqrt{\frac{\gamma+1}{2}}\end{pmatrix}, \tag{2.21}$$

which takes $\boldsymbol{\Psi}(x,t)$ to $\boldsymbol{\Psi}'(x',t')$ under the Lorentz transformation (2.19), *i.e.*

$$\boldsymbol{\Psi}'(x',t')=\boldsymbol{S}\boldsymbol{\Psi}(x,t), \tag{2.22}$$

where $\mathrm{sign}(x)$ is the sign function which returns 1 if $x>0$, 0 if $x=0$, and -1 if $x<0$.

Applying the transformation (2.22) with (2.21) to the standing wave solution (2.17) gives another solution of the NLD Eqs. (2.1)–(2.5), *i.e.* the moving wave solution

$$\boldsymbol{\Psi}^{\mathrm{mw}}(x-x_0,t)=\begin{pmatrix}\sqrt{\frac{\gamma+1}{2}}\psi_1^{\mathrm{sw}}(x',t')+\mathrm{sign}(V)\sqrt{\frac{\gamma-1}{2}}\psi_2^{\mathrm{sw}}(x',t')\\ \mathrm{sign}(V)\sqrt{\frac{\gamma-1}{2}}\psi_1^{\mathrm{sw}}(x',t')+\sqrt{\frac{\gamma+1}{2}}\psi_2^{\mathrm{sw}}(x',t')\end{pmatrix}. \tag{2.23}$$

This solution represents a NLD solitary wave with velocity V and will return to the standing wave (2.17) if setting $V=0$ and $x_0=0$.

2.4. Time reversibility

This subsection will show that the NLD Eq. (2.1) with L_{I} given in (2.5) remains invariant under the time reversal operation

$$x'=x,\quad t'=-t,\quad \boldsymbol{\Psi}'(x',t')=\boldsymbol{K}\boldsymbol{\Psi}(x,t),\quad \boldsymbol{K}=\boldsymbol{\gamma}^0\mathcal{C}, \tag{2.24}$$

where $\mathcal{C}$ denotes the complex conjugate operation on $\boldsymbol{\Psi}(x,t)$, *i.e.* $\boldsymbol{\Psi}^*(x,t)=\mathcal{C}\boldsymbol{\Psi}(x,t)$, the time-reversal operator $\boldsymbol{K}$ satisfies

$$\boldsymbol{K}^{\dagger}\boldsymbol{K}=\boldsymbol{I},\quad \boldsymbol{K}\gamma^0=\gamma^0\boldsymbol{K},\quad \boldsymbol{K}\gamma^1=-\gamma^1\boldsymbol{K}, \tag{2.25}$$

due to the anticommutation relation $\{\gamma^\mu,\gamma^\nu\}=2\eta^{\mu\nu}\boldsymbol{I}$, and $\boldsymbol{I}$ is the unit matrix. From the relations (2.25), it can be easily verified that

$$\begin{aligned}&(\bar{\Psi}'\Psi')(x',t')=(\bar{\Psi}\Psi)(x,t),\\&(\bar{\Psi}'\gamma^0\Psi')(x',t')=(\bar{\Psi}\gamma^0\Psi)(x,t),\\&(\bar{\Psi}'\gamma^1\Psi')(x',t')=-(\bar{\Psi}\gamma^1\Psi)(x,t),\end{aligned} \tag{2.26}$$

so that the self-interaction Lagrangian in (2.5) satisfies

$$L_{\mathrm{I}}'[\Psi'](x',t')=L_{\mathrm{I}}[\Psi](x,t), \tag{2.27}$$

under the time reversal transformation (2.24).

Applying the time-reversal operator $\boldsymbol{K}$ to the NLD Eq. (2.18) and using the definition (2.24) as well as the relations (2.25) and (2.27) lead to an equation which has the same form as shown in (2.20). That is, if a spinor $\Psi(x,t)$ satisfies the NLD Eq. (2.18), then the transformed spinor $\Psi'(x',t')$ by the time reversal operation (2.24) will also satisfy the same NLD equation, *i.e.* the NLD Eq. (2.18) is time reversible under the operation (2.24).

3. Numerical methods

As we mentioned in Section 1, some numerical methods have been well developed for the NLD equation with a scalar or vector self-interaction. This section will extendedly present and compare several numerical methods for solving the (1 + 1)-dimensional NLD Eq. (3.1) with the general scalar and vector self-interaction (2.5). Their numerical analyzes will be presented in Section 4.

For the sake of convenience, divide the bounded spatial domain $\Omega\subset\mathbb{R}$ into a uniform partition $\{x_j|x_j=jh\in\Omega,j\in\mathbb{Z}\}$ with a constant stepsize $h>0$ and give a grid in time $\{t_n=n\tau,n=0,1,\ldots\}$ with a time stepsize $\tau>0$, and recast the NLD Eq. (2.18) into

$$\frac{\partial\Psi}{\partial t}+\gamma^0\gamma^1\frac{\partial\Psi}{\partial x}+\mathtt{i}m\gamma^0\Psi-\mathtt{i}f_{\mathrm{s}}\gamma^0\Psi-\mathtt{i}f_{\mathrm{v}}\bar{\Psi}\gamma_\mu\Psi\gamma^0\gamma^\mu\Psi=0, \tag{3.1}$$

where

$$f_{\mathrm{s}}:=s(k+1)w_{\mathrm{s}}^k,\quad w_{\mathrm{s}}:=\bar{\Psi}\Psi,\quad f_{\mathrm{v}}:=v(k+1)w_{\mathrm{v}}^{(k-1)/2},\quad w_{\mathrm{v}}:=\bar{\Psi}\gamma^\nu\Psi\bar{\Psi}\gamma_\nu\Psi,$$

all of which are real functions, and the dependence of $\Psi(x,t)$ on (x,t) is implied.

3.1. Several finite difference schemes

Use Ψ_j^n to denote approximation of $\Psi(x_j,t_n)$ and define the forward, backward and centered difference operators in space and time by:

$$\begin{aligned}&\delta_t^{\pm}=\pm(E_t^{\pm1}-I)/\tau,\quad \delta_t^0=(E_t-E_t^{-1})/2\tau,\\&\delta_x^{\pm}=\pm(E_x^{\pm1}-I)/h,\quad \delta_x^0=(E_x-E_x^{-1})/2h,\end{aligned} \tag{3.2}$$

where I is the identity operator, and E_t and E_x are the translation operators in time and space, respectively, defined by

$$E_t\Psi_j^n:=\Psi_j^{n+1},\quad E_x\Psi_j^n:=\Psi_{j+1}^n,$$

whose inverses exist and are defined by

$$E_t^{-1}\Psi_j^n:=\Psi_j^{n-1},\quad E_x^{-1}\Psi_j^n:=\Psi_{j-1}^n.$$

Besides, several symbols are also introduced for arithmetic averaging operators:

$$\ell_t^{\pm}\Psi_j^n:=\frac{1}{2}(\Psi_j^{n\pm1}+\Psi_j^n),\quad \ell_t^0\Psi_j^n:=\frac{1}{2}(\Psi_j^{n+1}+\Psi_j^{n-1}),$$

$$\ell_x^{\pm}\Psi_j^n:=\frac{1}{2}(\Psi_{j\pm1}^n+\Psi_j^n),\quad \ell_x^0\Psi_j^n:=\frac{1}{2}(\Psi_{j+1}^n+\Psi_{j-1}^n)$$

and for an extrapolation operator:

$$\ell_t^{\mathrm{e}}\Psi_j^n=\frac{3}{2}\Psi_j^n-\frac{1}{2}\Psi_j^{n-1}.$$

- **Crank–Nicolson schemes** The CN scheme and its linearized version have been studied in [48,53,54] for the NLD equation with the quadric scalar self-interaction. For the system (3.1), the extension of the CN scheme in [54,62] may be written as

$$\delta_t^+\Psi_j^n+\gamma^0\gamma^1\ell_t^+\delta_x^0\Psi_j^n+\mathrm{i}m\gamma^0\ell_t^+\Psi_j^n-\mathrm{i}\frac{\delta_t^+(F_s)_j^n}{\delta_t^+(w_s)_j^n}\gamma^0\ell_t^+\Psi_j^n-\mathrm{i}\frac{\delta_t^+(F_v)_j^n}{\delta_t^+(w_v)_j^n}\ell_t^+(\bar{\Psi}\gamma_\mu\Psi)_j^n\gamma^0\gamma^\mu\ell_t^+\Psi_j^n=0, \tag{3.3}$$

by approximating (3.1) at point $(x_j,t_{n+\frac{1}{2}})$ with compact central difference quotient in place of the partial derivative, where

$$F_I(w_I):=\int_0^{w_I}f_I(x)\mathrm{d}x,\quad I=\mathrm{s},\mathrm{v}.$$

The above CN scheme (named as CN hereafter) is fully implicit and forms a nonlinear algebraic system. In practice, the linearization technique is often used to overcome difficulty in directly solving such nonlinear algebraic system. Two linearization techniques [62] for numerical methods of the nonlinear Schrödinger equation are borrowed here. The first linearized CN scheme we consider is using wholly the extrapolation technique to the nonlinear self-interaction terms in (3.1)

$$\delta_t^+\Psi_j^n+\gamma^0\gamma^1\ell_t^+\delta_x^0\Psi_j^n+\mathrm{i}m\gamma^0\ell_t^+\Psi_j^n-\mathrm{i}\ell_t^e\left(f_s\gamma^0\Psi+f_v\bar{\Psi}\gamma_\mu\Psi\gamma^0\gamma^\mu\Psi\right)_j^n=0, \tag{3.4}$$

which will be called by LCN1. The second linearized CN scheme, denoted by LCN2, is

$$\delta_t^+\Psi_j^n+\gamma^0\gamma^1\ell_t^+\delta_x^0\Psi_j^n+\mathrm{i}m\gamma^0\ell_t^+\Psi_j^n-\mathrm{i}\ell_t^e(f_s)_j^n\gamma^0\ell_t^+\Psi_j^n-\mathrm{i}\ell_t^e(f_v\bar{\Psi}\gamma_\mu\Psi)_j^n\gamma^0\gamma^\mu\ell_t^+\Psi_j^n=0, \tag{3.5}$$

by partially applying the extrapolation technique to the nonlinear self-interaction terms. It is worth noting that the above linearized CN schemes are not linearized version of the CN scheme (3.3). The LCN2 scheme may conserve the charge and behaves better than the LCN1 scheme (*vide post*).

Remark 3.1. For the (1 + 1)-dimensional NLD Eq. (2.1) with the quadric scalar self-interaction Lagrangian (2.3), the CN scheme (named by CNO) proposed in [48] is

$$\delta_t^+\Psi_j^n+\gamma^0\gamma^1\ell_t^+\delta_x^0\Psi_j^n+\mathrm{i}m\gamma^0\ell_t^+\Psi_j^n-2\mathrm{i}s(\ell_t^+\bar{\Psi}_j^n\ell_t^+\Psi_j^n)\gamma^0\ell_t^+\Psi_j^n=0, \tag{3.6}$$

and its linearized version (called by LCNO) is given in [53] as follows

$$\delta_t^+\Psi_j^n+\gamma^0\gamma^1\ell_t^+\delta_x^0\Psi_j^n+\mathrm{i}m\gamma^0\ell_t^+\Psi_j^n-2\mathrm{i}s\left((\bar{\Psi}\Psi)_j^n-\tau\mathrm{Re}(\bar{\Psi}_j^n\gamma^0\gamma^1\delta_x^0\Psi_j^n)\right)\gamma^0\ell_t^+\Psi_j^n=0. \tag{3.7}$$

We will show in Section 4 that the CN, CNO and LCNO schemes conserve the charge and the CN scheme further conserves the energy.

- **Odd–even hopscotch scheme.** The odd–even hopscotch scheme is a numerical integration technique for time-dependent partial differential equations, see [63]. Its key point is that the forward Euler-central difference scheme is used for the odd grid points while at the even points the backward Euler-central difference scheme is recovered. Thus the odd–even hopscotch scheme may be explicitly implemented. Such scheme applied to the system (3.1) becomes

$$\delta_t^+\Psi_j^n+\gamma^0\gamma^1\delta_x^0\Psi_j^n+\mathrm{i}m\gamma^0\Psi_j^n-\mathrm{i}\ell_x^0\left(f_s\gamma^0\Psi+f_v\bar{\Psi}\gamma_\mu\Psi\gamma^0\gamma^\mu\Psi\right)_j^n=0,\quad n+j\text{ is odd}, \tag{3.8}$$

$$\delta_t^-\Psi_j^{n+1}+\gamma^0\gamma^1\delta_x^0\Psi_j^{n+1}+\mathrm{i}m\gamma^0\Psi_j^{n+1}-\mathrm{i}\ell_x^0\left(f_s\gamma^0\Psi+f_v\bar{\Psi}\gamma_\mu\Psi\gamma^0\gamma^\mu\Psi\right)_j^{n+1}=0,\quad n+j\text{ is even}. \tag{3.9}$$

In the following we will call it by HS.

- **Leapfrog scheme.** The leapfrog scheme looks quite similar to the forward scheme, see *e.g.* (3.8), except it uses the values from the previous time-step instead of the current one. For the system (3.1), it is

$$\delta_t^0\Psi_j^n+\gamma^0\gamma^1\delta_x^0\Psi_j^n+\mathrm{i}m\gamma^0\Psi_j^n-\mathrm{i}\left(f_s\gamma^0\Psi+f_v\bar{\Psi}\gamma_\mu\Psi\gamma^0\gamma^\mu\Psi\right)_j^n=0, \tag{3.10}$$

which is a three-level explicit scheme in time with a central difference in space and will be named by LF.

- **Semi-implicit scheme.** Another three-level scheme considered here for the system (3.1) is

$$\delta_t^0\Psi_j^n+\gamma^0\gamma^1\ell_t^0\delta_x^0\Psi_j^n+\mathrm{i}m\gamma^0\ell_t^0\Psi_j^n-\mathrm{i}\left(f_s\gamma^0\Psi+f_v\bar{\Psi}\gamma_\mu\Psi\gamma^0\gamma^\mu\Psi\right)_j^n=0, \tag{3.11}$$

which is obtained by approximating explicitly the nonlinear terms but implicitly the linear terms and will be called by SI. It is worth noting that such semi-implicit scheme has been studied for the NLD equation with the quadric scalar self-interaction in [46].

3.2. Exponential operator splitting scheme

This subsection goes into discussing exponential operator splitting scheme for the NLD Eq. (3.1). For convenience, we rewrite the system (3.1) as follows

$$\boldsymbol{\Psi}_t = (\mathcal{L} + \mathcal{N}_{\mathrm{s}} + \mathcal{N}_{\mathrm{v}})\boldsymbol{\Psi}, \tag{3.12}$$

where the linear operator $\mathcal{L}$ and both nonlinear operators $\mathcal{N}_{\mathrm{s}}$ and $\mathcal{N}_{\mathrm{v}}$ are defined by

$$\mathcal{L}\boldsymbol{\Psi} := -\boldsymbol{\gamma}^0\boldsymbol{\gamma}^1\boldsymbol{\Psi}_x - \mathrm{i}m\boldsymbol{\gamma}^0\boldsymbol{\Psi}, \quad \mathcal{N}_{\mathrm{s}}\boldsymbol{\Psi} := \mathrm{i}f_{\mathrm{s}}\boldsymbol{\gamma}^0\boldsymbol{\Psi}, \quad \mathcal{N}_{\mathrm{v}}\boldsymbol{\Psi} := \mathrm{i}f_{\mathrm{v}}\bar{\boldsymbol{\Psi}}\boldsymbol{\gamma}_\mu\boldsymbol{\Psi}\boldsymbol{\gamma}^0\boldsymbol{\gamma}^\mu\boldsymbol{\Psi}.$$

Then the problem (3.12) may be decomposed into three subproblems as follows

$$\boldsymbol{\Psi}_t = \mathcal{L}\boldsymbol{\Psi}, \tag{3.13}$$
$$\boldsymbol{\Psi}_t = \mathcal{N}_{\mathrm{s}}\boldsymbol{\Psi}, \tag{3.14}$$
$$\boldsymbol{\Psi}_t = \mathcal{N}_{\mathrm{v}}\boldsymbol{\Psi}. \tag{3.15}$$

Due to the local conservation laws which are discussed in Section 3.2.2, solutions of the nonlinear subproblem (3.14) or (3.15) may be expressed as an exponential of the operator $\mathcal{N}_{\mathrm{s}}$ or $\mathcal{N}_{\mathrm{v}}$ acting on "initial data". Thus we may introduce the exponential operator splitting scheme for the the NLD Eq. (3.12) or (3.1), imitating that for the linear partial differential equations, see *e.g.* [64,65] and references therein. Based on the exact or approximate solvers of those three subproblems, a more general K-stage Nth order exponential operator splitting method [66,67] for the system (3.12) can be cast into product of finitely many exponentials as follows

$$\boldsymbol{\Psi}_j^{n+1} = \prod_{i=1}^{K}\Big(\exp(\tau_i\mathcal{A}_i^{(1)})\exp(\tau_i\mathcal{A}_i^{(2)})\exp(\tau_i\mathcal{A}_i^{(3)})\Big)\boldsymbol{\Psi}_j^n, \tag{3.16}$$

where τ_i denotes the time stepsize used within the i-th stage and satisfies $\sum_{i=1}^{K}\tau_i = \tau$, and $\{\mathcal{A}_i^{(1)}, \mathcal{A}_i^{(2)}, \mathcal{A}_i^{(3)}\}$ is any permutation of $\{\mathcal{L}, \mathcal{N}_{\mathrm{s}}, \mathcal{N}_{\mathrm{v}}\}$. Hereafter we call the operator splitting scheme (3.16) by `OS(N)`. Although one single product of finitely many exponentials exponentials (3.16) is employed here, it should be pointed out that the linear combination of such finite products can also be used to construct exponential operator splitting schemes as shown in [64].

A simple example is the well-known second-order accurate operator splitting method of Strang (named by `OS(2)`) with

$$K = 2, \quad \tau_1 = \tau_2 = \frac{1}{2}\tau, \quad \mathcal{A}_1^{(1)} = \mathcal{A}_2^{(3)}, \quad \mathcal{A}_1^{(3)} = \mathcal{A}_2^{(1)}, \quad \mathcal{A}_1^{(2)} = \mathcal{A}_2^{(2)}. \tag{3.17}$$

Another example is the fourth-order accurate operator splitting method [66] with

$$K = 8, \quad \mathcal{A}_q^{(1)} = \mathcal{A}_p^{(3)}, \quad \mathcal{A}_q^{(3)} = \mathcal{A}_p^{(1)}, \quad \mathcal{A}_q^{(2)} = \mathcal{A}_p^{(2)}, \quad q = 1,4,6,7, \quad p = 2,3,5,8,$$

$$\tau_1 = \tau_8 = \frac{\tau}{5 - \sqrt{13} + \sqrt{2(1+\sqrt{13})}}, \quad \tau_2 = \tau_7 = \frac{7 + \sqrt{13} - \sqrt{2(1+\sqrt{13})}}{24}\tau,$$

$$\tau_3 = \tau_6 = \frac{\tau_1^2}{\tau_2 - \tau_1}, \quad \tau_4 = \tau_5 = \frac{\tau_2(\tau_1 - \tau_2)}{3\tau_1 - 2\tau_2},$$

which is denoted by `OS(4)` in the following.

Remark 3.2. Another operator splitting scheme is studied in [52] for the NLD Eq. (2.1) but only with the quadric scalar self-interaction Lagrangian, and the second-order accurate Strang method (3.17) is applied there. For the system (3.1), it is based on the following operator decomposition

$$\boldsymbol{\Psi}_t = \Big(\hat{\mathcal{L}} + \hat{\mathcal{N}}_{\mathrm{s}} + \hat{\mathcal{N}}_{\mathrm{v}}\Big)\boldsymbol{\Psi}, \tag{3.18}$$

with

$$\hat{\mathcal{L}}\boldsymbol{\Psi} := -\boldsymbol{\gamma}^0\boldsymbol{\gamma}^1\boldsymbol{\Psi}_x, \quad \hat{\mathcal{N}}_{\mathrm{s}}\boldsymbol{\Psi} := -\mathrm{i}(m - f_{\mathrm{s}})\boldsymbol{\gamma}^0\boldsymbol{\Psi}, \quad \hat{\mathcal{N}}_{\mathrm{v}}\boldsymbol{\Psi} := \mathrm{i}f_{\mathrm{v}}\bar{\boldsymbol{\Psi}}\boldsymbol{\gamma}_\mu\boldsymbol{\Psi}\boldsymbol{\gamma}^0\boldsymbol{\gamma}^\mu\boldsymbol{\Psi}.$$

Remark 3.3. For the linear parabolic equation which is an irreversible system, a more general exponential operator splitting scheme and its accuracy as well as stability are discussed in [64], based on linear combinations of products of finitely many exponentials. It is shown that for such irreversible system, negative weights or negative time stepsizes τ_i may lead to instability; and the highest order of the stable exponential operator splitting approximation (only with positive weights and positive sub-stepsizes in time) is two. However, for time-reversible systems, such as the Hamilton system, the Schrödinger equations and the NLD Eq. (2.1) with L_{I} given in (2.5), it is immaterial whether or not the weights or time stepsizes τ_i are

positive [65], where a general framework was presented for understanding the structure of the exponential operator splitting schemes and both specific error terms and order conditions were analytically solved.

3.2.1. Linear subproblem

We are now solving the linear subproblem (3.13). Denote its "initial data" by $\mathbf{\Psi}_j^{(0)} = \left((\psi_1)_j^{(0)}, (\psi_2)_j^{(0)}\right)^T$ at the ith stage in (3.16).

If the spinor $\mathbf{\Psi}$ is periodic (*e.g.* 2π-periodic) with respect to x, the Fourier spectral method is employed to solve (3.13) and gives

$$\mathbf{\Psi}_j^{(1)} = \mathcal{F}^{-1}\left(\exp\left(-\mathrm{i}\tau_i(\kappa\boldsymbol{\gamma}^0\boldsymbol{\gamma}^1 + m\boldsymbol{\gamma}^0)\right)\mathcal{F}\left(\mathbf{\Psi}_j^{(0)}\right)\right). \tag{3.19}$$

Here $\mathcal{F}$ and $\mathcal{F}^{-1}$ denote the discrete Fourier transform operator and its inverse, respectively, defined by

$$\left(\mathcal{F}(\mathbf{\Psi})\right)_\kappa := \sum_{j=0}^{J-1}\mathbf{\Psi}_j \exp\left(-\mathrm{i}2\pi\kappa\frac{j}{J}\right) \quad \kappa = 0,\ldots,J-1,$$

$$\left(\mathcal{F}^{-1}(\mathbf{\Phi})\right)_j := \frac{1}{J}\sum_{\kappa=0}^{J-1}\mathbf{\Phi}_\kappa \exp\left(\mathrm{i}2\pi j\frac{\kappa}{J}\right) \quad j = 0,\ldots,J-1,$$

where J is the grid point number, and the matrix exponential in (3.19) can be easily evaluated as follows

$$\exp\left(-\mathrm{i}\tau_i(\kappa\boldsymbol{\gamma}^0\boldsymbol{\gamma}^1 + m\boldsymbol{\gamma}^0)\right) = \begin{pmatrix} \cos(\zeta\tau_i) - \mathrm{i}\frac{m}{\zeta}\sin(\zeta\tau_i) & -\mathrm{i}\frac{\kappa}{\zeta}\sin(\zeta\tau_i) \\ -\mathrm{i}\frac{\kappa}{\zeta}\sin(\zeta\tau_i) & \cos(\zeta\tau_i) + \mathrm{i}\frac{m}{\zeta}\sin(\zeta\tau_i) \end{pmatrix}, \tag{3.20}$$

with $\zeta = \sqrt{\kappa^2 + m^2}$.

When the spinor $\mathbf{\Psi}$ is not periodic with respect to x, the fifth-order accurate finite difference WENO scheme will be used to solve the linear subproblem (3.13). The readers are referred to [68] for details. In this case, the linear subproblem (3.13) can also be solved by using the characteristics method.

3.2.2. Nonlinear subproblems

The nonlinear subproblems (3.14) and (3.15) are left to be solved now. Their "initial data" is still denoted by $\mathbf{\Psi}_j^{(0)} = \left((\psi_1)_j^{(0)}, (\psi_2)_j^{(0)}\right)^T$ at the i-th stage in (3.16), and define

$$t_n^{(i)} = t_n + \sum_{p=1}^{i-1}\tau_p, \quad i = 1,2,\ldots,K.$$

For nonlinear subproblem (3.14), it is not difficulty to verify that $\partial_t w_s = 0$ so that

$$\partial_t f_s = 0. \tag{3.21}$$

Using this local conservation law gives the solution at $t = t_n^{(i+1)}$ of (3.14) with the "initial data" $\mathbf{\Psi}_j^{(0)}$ as follows

$$\mathbf{\Psi}_j^{(1)} = \exp\left(\mathrm{i}\int_{t_n^{(i)}}^{t_n^{(i+1)}}(f_s)_j\boldsymbol{\gamma}^0\mathrm{d}t\right)\mathbf{\Psi}_j^{(0)} = \exp\left(\mathrm{i}(f_s)_j^{(0)}\boldsymbol{\gamma}^0\tau_i\right)\mathbf{\Psi}_j^{(0)} = \mathrm{diag}\left\{\exp\left(\mathrm{i}(f_s)_j^{(0)}\tau_i\right), \exp\left(-\mathrm{i}(f_s)_j^{(0)}\tau_i\right)\right\}\mathbf{\Psi}_j^{(0)}. \tag{3.22}$$

For the nonlinear subproblem (3.15), one may still similarly derive the following local conservation laws

$$\partial_t(\bar{\mathbf{\Psi}}\boldsymbol{\gamma}_0\mathbf{\Psi}) = 0, \quad \partial_t(\bar{\mathbf{\Psi}}\boldsymbol{\gamma}_1\mathbf{\Psi}) = 0, \quad \partial_t f_v = 0. \tag{3.23}$$

by direct algebraic manipulations if using the fact that $\bar{\mathbf{\Psi}}\boldsymbol{\gamma}_0\mathbf{\Psi}$, $\bar{\mathbf{\Psi}}\boldsymbol{\gamma}_1\mathbf{\Psi}$ and f_v are all real. Consequently, integrating (3.15) from $t_n^{(i)}$ to $t_n^{(i+1)}$ gives its solution as follows

$$\mathbf{\Psi}_j^{(1)} = \exp\left(\mathrm{i}(f_v\bar{\mathbf{\Psi}}\boldsymbol{\gamma}_\mu\mathbf{\Psi})_j^{(0)}\boldsymbol{\gamma}^0\boldsymbol{\gamma}^\mu\tau_i\right)\mathbf{\Psi}_j^{(0)} = \exp(\mathrm{i}\alpha\tau_i)\begin{pmatrix}\cos(\beta\tau_i) & \mathrm{i}\sin(\beta\tau_i) \\ \mathrm{i}\sin(\beta\tau_i) & \cos(\beta\tau_i)\end{pmatrix}\mathbf{\Psi}_j^{(0)}, \tag{3.24}$$

where $\alpha = (f_v\bar{\mathbf{\Psi}}\boldsymbol{\gamma}_0\mathbf{\Psi})_j^{(0)}$ and $\beta = (f_v\bar{\mathbf{\Psi}}\boldsymbol{\gamma}_1\mathbf{\Psi})_j^{(0)}$.

Remark 3.4. It is because the local conservation laws (3.21) and (3.23) are fully exploited here that we can solve exactly the nonlinear subproblems (3.14) and (3.15) which imply the more higher accuracy of the OS method than that of other methods.

In summary, we have.

- The `CN` (3.3) and `CNO` (3.6) schemes are nonlinear and implicit, and could be solved by iterative algorithms such as Picard iteration and Newton method.
- The `LCNO` (3.7), `LCN1` (3.4), `LCN2` (3.5) and `SI` (3.11) schemes are linear and implicit.

- The HS (3.8), (3.9), LF (3.10), and OS(N) (3.16) schemes are explicit.

4. Numerical analysis

Before investigating the performance of the numerical methods proposed in Section 3, this section will go first into numerical analysis of them, including the accuracy in the sense of the truncation error, time reversibility and the conservation of the charge or energy.

Proposition 4.1. *If $\Psi(x,t) \in C^\infty(\mathbb{R}\times[0,+\infty))$ is periodic, then the* CN, CNO, LCNO, LCN1, LCN2, HS, LF *and* SI *schemes are of order $\mathcal{O}(\tau^2+h^2)$, and the* OS(N) *scheme is of order $\mathcal{O}(\tau^N+h^m)$ for any arbitrary large $m>0$.*

Proof. The proof is very straightforward by using directly the Taylor series expansion for the finite difference schemes and the Fourier spectral analysis for the OS(N) scheme, and thus is skipped here for saving space. □

Proposition 4.2. *The* CN, CNO, HS, LF, SI, *and* OS(N) *schemes are time reversible, but the* LCNO, LCN1, LCN2 *schemes are not.*

Proof. We give the proof for the CN and LCN1 schemes as an example and the others can be proved in a similar way.

According to the transformation (2.24), the relation between the transformed finite difference solution and the original one should be $(\Psi')_j^{n'} = \boldsymbol{K}\Psi_j^n = (\boldsymbol{K}\Psi)_j^n$ with $n' = -n$. Consequently, we have

$$\begin{aligned}
&\boldsymbol{K}\delta_t^+\Psi_j^n = \boldsymbol{K}\tfrac{\Psi_j^{n+1}-\Psi_j^n}{\tau} = \tfrac{(\Psi')_j^{n'-1}-(\Psi')_j^{n'}}{\tau} = -\delta_t^+(\Psi')_j^{n'-1},\\
&\boldsymbol{K}\ell_t^+\Psi_j^n = \boldsymbol{K}\tfrac{\Psi_j^{n+1}+\Psi_j^n}{2} = \tfrac{(\Psi')_j^{n'-1}+(\Psi')_j^{n'}}{2} = \ell_t^+(\Psi')_j^{n'-1}
\end{aligned} \tag{4.1}$$

and then using the relations in (2.26) yields

$$\begin{aligned}
&\ell_t^+(\bar\Psi\gamma_0\Psi)_j^n = \ell_t^+(\bar\Psi'\gamma_0\Psi')_j^{n'-1},\\
&\ell_t^+(\bar\Psi\gamma_1\Psi)_j^n = -\ell_t^+(\bar\Psi'\gamma_1\Psi')_j^{n'-1},\\
&\delta_t^+(w_I)_j^n = -\delta_t^+(w_I')_j^{n'-1},\\
&\delta_t^+(F_I)_j^n = -\delta_t^+(F_I')_j^{n'-1}
\end{aligned} \tag{4.2}$$

for $I\in\{\mathrm{s},\mathrm{v}\}$. Applying the time-reversal operator K to the CN scheme (3.3) and using the commutation relation (2.25) and Eqs. (4.1) and (4.2) lead to

$$\delta_t^+(\Psi')_j^{n'-1} + \gamma^0\gamma^1\ell_t^+\delta_x^0(\Psi')_j^{n'-1} + \mathrm{i}m\gamma^0\ell_t^+(\Psi')_j^{n'-1} - \mathrm{i}\frac{\delta_t^+(F_\mathrm{s}')_j^{n'-1}}{\delta_t^+(w_\mathrm{s}')_j^{n'-1}}\gamma^0\ell_t^+(\Psi')_j^{n'-1} - \mathrm{i}\frac{\delta_t^+(F_\mathrm{v}')_j^{n'-1}}{\delta_t^+(w_\mathrm{v}')_j^{n'-1}}\ell_t^+(\bar\Psi'\gamma_\mu\Psi')_j^{n'-1}\gamma^0\gamma^\mu\ell_t^+(\Psi')_j^{n'-1} = 0,$$

which is exactly the CN scheme (3.3) applied to $(\Psi')_j^{n'-1}$. That is, the CN scheme is invariant under the time-reversal transformation, namely, it is time reversible.

The fact that the LCN1 scheme (3.4) is not time reversible can be observed directly if noting

$$\begin{aligned}
-\boldsymbol{K}\,\mathrm{i}\ell_t^\mathrm{e}\left(f_\mathrm{s}\gamma^0\Psi + f_\mathrm{v}\bar\Psi\gamma_\mu\Psi\gamma^0\gamma^\mu\Psi\right)_j^n &= \mathrm{i}\left[\frac{3}{2}\left(f_\mathrm{s}'\gamma^0\Psi' + f_\mathrm{v}'\bar\Psi'\gamma_\mu\Psi'\gamma^0\gamma^\mu\Psi'\right)_j^{n'} - \frac{1}{2}\left(f_\mathrm{s}'\gamma^0\Psi' + f_\mathrm{v}'\bar\Psi'\gamma_\mu\Psi'\gamma^0\gamma^\mu\Psi'\right)_j^{n'+1}\right]\\
&\neq \mathrm{i}\ell_t^\mathrm{e}\left(f_\mathrm{s}'\gamma^0\Psi' + f_\mathrm{v}'\bar\Psi'\gamma_\mu\Psi'\gamma^0\gamma^\mu\Psi'\right)_j^{n'-1}. \qquad \square
\end{aligned}$$

Next, we will discuss the conservation of the discrete energy, linear momentum and charge defined below for the numerical methods given in Section 3. After performing the integration in the computational domain $\Omega=[x_\mathrm{L},x_\mathrm{R}]$ and then approximating the first derivative operator ∂_x with the centered difference operator δ_x^0 as well as the integral operator $\int_{x_\mathrm{L}}^{x_\mathrm{R}}\mathrm{d}x$ with the summation operator $h\sum_{j=1}^J$ in Eq. (2.8), we have the discrete energy, linear momentum and charge at the nth time step

$$\begin{aligned}
&E_h^n = h\sum_{j=1}^J\left(\mathrm{Im}(\bar\Psi\gamma^1\delta_x^0\Psi) + m(\bar\Psi\Psi) - F_\mathrm{s} - \tfrac{1}{2}F_\mathrm{v}\right)_j^n,\\
&P_h^n = h\sum_{j=1}^J\mathrm{Im}(\Psi^\dagger\delta_x^0\Psi)_j^n,\\
&Q_h^n = \|\Psi^n\|^2 := \langle\Psi^n,\Psi^n\rangle = h\sum_{j=1}^J(\Psi_j^n)^\dagger\Psi_j^n,
\end{aligned}$$

where the inner product $\langle\cdot,\cdot\rangle$ is defined as

$$\langle \mathtt{u}, \mathtt{v}\rangle = h\sum_{j=1}^{J}(\mathtt{u}_j)^{\dagger}\mathtt{v}_j$$

for two complex-valued vectors $\mathtt{u}$ and $\mathtt{v}$, and J is the grid point number. Here the values of $\boldsymbol{\Psi}$ at x_j with $1\leqslant j\leqslant J$ are unknowns and those at x_0 and x_{J+1} are determined by appropriate boundary conditions.

We first present the following lemma which can be verified through direct algebraic manipulations and will be used in discussing the conservation of the discrete charge, energy and linear momentum.

Lemma 4.3. *Given that $\boldsymbol{\Phi}_j^n$ is a complex-valued vector mesh function with two components evaluated at the mesh $\{x_j,t_n\}$ $(n=0,1,\cdots,N,j=0,1,\cdots,J+1)$ and a matrix $\boldsymbol{\Gamma}\in\{\boldsymbol{I}_2,\boldsymbol{\gamma}^0,\boldsymbol{\gamma}^1,\mathtt{i}\boldsymbol{\gamma}^0\boldsymbol{\gamma}^1\}$, we have the following identities*

(a) $2\mathrm{Re}\langle\ell_t^+\boldsymbol{\Phi}^n,\delta_t^+\boldsymbol{\Phi}^n\rangle=\delta_t^+\|\boldsymbol{\Phi}^n\|^2$;
(b) $2\mathrm{Re}\langle\boldsymbol{\gamma}^0\boldsymbol{\gamma}^1\delta_x^0\boldsymbol{\Phi}^n,\boldsymbol{\Phi}^n\rangle=\frac{1}{2}(\bar{\boldsymbol{\Phi}}_{J+1}^n\boldsymbol{\gamma}^1\boldsymbol{\Phi}_J^n+\bar{\boldsymbol{\Phi}}_J^n\boldsymbol{\gamma}^1\boldsymbol{\Phi}_{J+1}^n)-\frac{1}{2}(\bar{\boldsymbol{\Phi}}_1^n\boldsymbol{\gamma}^1\boldsymbol{\Phi}_0^n+\bar{\boldsymbol{\Phi}}_0^n\boldsymbol{\gamma}^1\boldsymbol{\Phi}_1^n)$;
(c) $\mathrm{Im}\left(\ell_t^+\bar{\boldsymbol{\Phi}}_j^n\boldsymbol{\Gamma}\ell_t^+\boldsymbol{\Phi}_j^n\right)=0$;
(d) $2\mathrm{Re}(\delta_t^+\bar{\boldsymbol{\Phi}}_j^n\boldsymbol{\Gamma}\ell_t^+\boldsymbol{\Phi}_j^n)=\delta_t^+(\bar{\boldsymbol{\Phi}}_j^n\boldsymbol{\Gamma}\boldsymbol{\Phi}_j^n)$;
(e)
$$2\mathtt{i}\mathrm{Im}\langle\boldsymbol{\gamma}^0\boldsymbol{\gamma}^1(\ell_t^+\delta_x^0)\boldsymbol{\Phi}^n,\delta_t^+\boldsymbol{\Phi}^n\rangle=-\delta_t^+\left(h\textstyle\sum_{j=1}^{J}(\bar{\boldsymbol{\Phi}}_j^n\boldsymbol{\gamma}^1\delta_x^0\boldsymbol{\Phi}_j^n)\right)+\frac{1}{2}\left((\ell_t^+\bar{\boldsymbol{\Phi}}_{J+1}^n\boldsymbol{\gamma}^1\delta_t^+\boldsymbol{\Phi}_J^n+\ell_t^+\bar{\boldsymbol{\Phi}}_J^n\boldsymbol{\gamma}^1\delta_t^+\boldsymbol{\Phi}_{J+1}^n)-(\ell_t^+\bar{\boldsymbol{\Phi}}_1^n\boldsymbol{\gamma}^1\delta_t^+\boldsymbol{\Phi}_0^n+\ell_t^+\bar{\boldsymbol{\Phi}}_0^n\boldsymbol{\gamma}^1\delta_t^+\boldsymbol{\Phi}_1^n)\right).$$

Proof. It can be checked that the following Leibniz rules

$$\delta_t^a(\mathtt{u}^{\dagger}\mathtt{v})_j^n=\delta_t^a(\mathtt{u}^{\dagger})_j^n\ell_t^a\mathtt{v}_j^n+\ell_t^a(\mathtt{u}^{\dagger})_j^n\delta_t^a\mathtt{v}_j^n$$

holds for any two spinors $\mathtt{u}(x,t),\mathtt{v}(x,t)$ and $a\in\{+,-,0\}$, and then we have

$$2\mathrm{Re}\langle\ell_t^+\boldsymbol{\Phi}^n,\delta_t^+\boldsymbol{\Phi}^n\rangle=\langle\delta_t^+\boldsymbol{\Phi}^n,\ell_t^+\boldsymbol{\Phi}^n\rangle+\langle\ell_t^+\boldsymbol{\Phi}^n,\delta_t^+\boldsymbol{\Phi}^n\rangle=h\sum_{j=1}^{J}\delta_t^+(\boldsymbol{\Phi}^{\dagger})_j^n\ell_t^+\boldsymbol{\Phi}_j^n+h\sum_{j=1}^{J}\ell_t^+(\boldsymbol{\Phi}^{\dagger})_j^n\delta_t^+\boldsymbol{\Phi}_j^n=h\sum_{j=1}^{J}\delta_t^+(\boldsymbol{\Phi}^{\dagger}\boldsymbol{\Phi})_j^n=\delta_t^+\|\boldsymbol{\Phi}^n\|^2.$$

Thus the identity (a) holds.

Because the operator $-\delta_x^0$ is the adjoint operator of δ_x^0 and $\boldsymbol{\gamma}^0\boldsymbol{\gamma}^1$ is an Hermite matrix, we get the identity (b) directly by rearranging the summation. The identity (c) can be easily verified if using the fact $(\boldsymbol{\gamma}^0\boldsymbol{\Gamma})^{\dagger}=\boldsymbol{\gamma}^0\boldsymbol{\Gamma}$. The proof of (d) (resp. (e)) is similar with that of (b) (resp. (c)). □

Proposition 4.4. *The* CN, CNO, LCNO, LCN2, *and* OS(N) *schemes conserve the discrete charge, but only the* CN *scheme conserves the discrete energy.*

Proof. We begin with the discrete conservation law of charge for the CN scheme (3.3). Performing the inner product of $\ell_t^+\boldsymbol{\Psi}^n$ and the CN scheme (3.3) leads to

$$\langle\ell_t^+\boldsymbol{\Psi}^n,\delta_t^+\boldsymbol{\Psi}^n\rangle+\langle\ell_t^+\boldsymbol{\Psi}^n,\boldsymbol{\gamma}^0\boldsymbol{\gamma}^1\delta_x^0\ell_t^+\boldsymbol{\Psi}^n\rangle+\langle\ell_t^+\boldsymbol{\Psi}^n,\mathtt{i}m\boldsymbol{\gamma}^0\ell_t^+\boldsymbol{\Psi}^n-\mathtt{i}\frac{\delta_t^+(F_{\mathrm{s}})^n}{\delta_t^+(w_{\mathrm{s}})^n}\boldsymbol{\gamma}^0\ell_t^+\boldsymbol{\Psi}^n\rangle+\langle\ell_t^+\boldsymbol{\Psi}^n,-\mathtt{i}\frac{\delta_t^+(F_{\mathrm{v}})^n}{\delta_t^+(w_{\mathrm{v}})^n}\ell_t^+(\bar{\boldsymbol{\Psi}}\boldsymbol{\gamma}_{\mu}\boldsymbol{\Psi})^n\boldsymbol{\gamma}^0\boldsymbol{\gamma}^{\mu}\ell_t^+\boldsymbol{\Psi}^n\rangle=0 \tag{4.3}$$

and then the conservation law of the discrete charge can be easily verified by taking directly the real part as follows

$$\delta_t^+Q_h^n=\frac{1}{2}(\ell_t^+\bar{\boldsymbol{\Psi}}_1^n\boldsymbol{\gamma}^1\ell_t^+\boldsymbol{\Psi}_0^n+\ell_t^+\bar{\boldsymbol{\Psi}}_0^n\boldsymbol{\gamma}^1\ell_t^+\boldsymbol{\Psi}_1^n)-\frac{1}{2}(\ell_t^+\bar{\boldsymbol{\Psi}}_{J+1}^n\boldsymbol{\gamma}^1\ell_t^+\boldsymbol{\Psi}_J^n+\ell_t^+\bar{\boldsymbol{\Psi}}_J^n\boldsymbol{\gamma}^1\ell_t^+\boldsymbol{\Psi}_{J+1}^n), \tag{4.4}$$

where Lemma 4.3 (a) is applied to the first term in Eq. (4.3), (b), to the second term and (c) to the third and fourth terms. Similarly, it can be verified that (4.4) holds for the CNO (3.6), LCNO (3.7) and LCN2 (3.5) schemes.

Performing the inner product of the CN scheme (3.3) and $\delta_t^+\boldsymbol{\Psi}^n$, keeping the imaginary part and applying Lemma 4.3 give directly the conservation of the discrete energy

$$\delta_t^+E_h^n=\frac{1}{2}\mathrm{Im}\left((\ell_t^+\bar{\boldsymbol{\Psi}}_{J+1}^n\boldsymbol{\gamma}^1\delta_t^+\boldsymbol{\Psi}_J^n+\ell_t^+\bar{\boldsymbol{\Psi}}_J^n\boldsymbol{\gamma}^1\delta_t^+\boldsymbol{\Psi}_{J+1}^n)-(\ell_t^+\bar{\boldsymbol{\Psi}}_1^n\boldsymbol{\gamma}^1\delta_t^+\boldsymbol{\Psi}_0^n+\ell_t^+\bar{\boldsymbol{\Psi}}_0^n\boldsymbol{\gamma}^1\delta_t^+\boldsymbol{\Psi}_1^n)\right).$$

For the Fourier spectral method (3.19), using the fact that $\exp(-\mathtt{i}\tau_i(\kappa\boldsymbol{\gamma}^0\boldsymbol{\gamma}^1+m\boldsymbol{\gamma}^0))$ in (3.20) is a unitary matrix yields

$$\left\|\exp\left(-\mathtt{i}\tau_i(\kappa\boldsymbol{\gamma}^0\boldsymbol{\gamma}^1+m\boldsymbol{\gamma}^0)\right)\boldsymbol{\Psi}_j^{(1)}\right\|^2=\left\|\boldsymbol{\Psi}_j^{(0)}\right\|^2$$

and then

$$\|\Psi^{(1)}\|^2 = \|\mathcal{F}^{-1}[\exp(-\mathrm{i}\tau_i(\kappa\gamma^0\gamma^1 + m\gamma^0))\mathcal{F}(\Psi^{(0)})]\|^2 = \|\exp(-\mathrm{i}\tau_i(\kappa\gamma^0\gamma^1 + m\gamma^0))\mathcal{F}(\Psi^{(0)})\|^2 = \|\mathcal{F}(\Psi^{(0)})\|^2 = \|\Psi^{(0)}\|^2,$$

where Parseval's identity is applied twice. It can be readily verified that the matrix exponents in Eqs. (3.22) and (3.24) are unitary, thus $\|\Psi^{(1)}\|^2 = \|\Psi^{(0)}\|^2$ holds both for Eqs. (3.22) and (3.24), *i.e.* Q_h should be conserved for solutions of the nonlinear subproblems. Therefore, the OS(N) scheme satisfies the conservation law of charge. □

Remark 4.1. It will be verified by numerical results in Section 5 that the LCN1, HS, LF and SI schemes do not conserve the discrete charge or energy, and none of the numerical methods presented in Section 3 conserves the discrete linear momentum.

5. Numerical results

This section will conduct numerical simulations to compare the performance of numerical schemes proposed in Section 3 and then utilize the OS(4) scheme to investigate the interaction dynamics for the NLD solitary waves (2.23) under the scalar and vector self-interaction. For those localized NLD solitary waves, the periodic boundary condition for the OS(N) scheme and the non-reflection boundary condition for other schemes could be adopted at the boundaries of the computational domain if a relatively large computational domain has been taken in our numerical experiments.

All calculations are performed on a Lenovo desktop computer with Intel Core i5 650 CPU and 4 GB RAM using double precision in the 3.0.0–24-generic x86_64 Linux operation system and the compiler is gcc 4.6.1. The computational domain Ω will be taken as $[-50, 50]$ in Examples 5.1–5.5 and $[-100, 100]$ in Example 5.6. and the particle mass m in Eq. (2.18) is chosen to be 1.

Example 5.1. The first example is devoted to comparing the numerical performance of all the numerical methods in Section 3 in terms of the accuracy, the conservativeness, the efficiency and the error growth. A one-humped solitary wave with the velocity $V = -0.2$ is simulated here under the quadric scalar self-interaction (*i.e.* $\upsilon = 0$ and $k = 1$), traveling from right to left with the parameters in (2.23): $x_0 = 5, s = 0.5$, and $\omega = 0.75$. The P^N-RKDG method [50] is also included here for comparison, which is assembled with a fourth-order accurate Runge–Kutta time discretization in time and the Legendre polynomials of degree at most N as local basis functions in the spatial Galerkin approximation.

Tables 1 and 2 summarize the numerical results at the final time $t = 50$, where err_2 and err_∞ are respectively the l^2 and l^∞ errors at the final time, $\mathcal{V}_Q, \mathcal{V}_E, \mathcal{V}_P$ measure respectively the variation of charge, energy and linear momentum at the final time relative to the initial quantities, and the CPU time of calculations with the same mesh size is recorded for comparing the efficiency. It can be observed clearly there that: (1) while the CN, CNO, LCNO, LCN1, LCN2, HS, LF, SI and OS(2) schemes are of the second-order accuracy, the OS(4), P^3-RKDG and P^4-RKDG methods exhibit at least the fourth-order accuracy; (2) The CN, CNO, LCNO, LCN2, OS(2) and OS(4) schemes conserve the discrete charge and only the CN scheme conserves the discrete energy, but none conserves the discrete linear momentum; (3) The OS(4) scheme could also keep very accurately the discrete energy and linear momentum with relatively fine meshes. All above numerical results are consistent with the theoretical results given in Section 4. Among the numerical methods of the second order accuracy, it is also found that the OS(2) scheme runs fastest (8.2 s for the mesh $\tau = 0.005$ and $h = 0.20$) if requiring to attain almost the same accuracy. Similarly, the OS(4) scheme runs much more faster than both P^3-RKDG and P^4-RKDG methods, and the ratio of the CPU time used by the OS(4) scheme over that used by the P^3-RKDG method is around 3.05%, and reduces to around 2.26% over that used by the P^4-RKDG method.

Fig. 1 plots the l^∞ error history in the finest mesh used in Tables 1 and 2. According to the curves shown there, it can be seen there that the l^∞ error of all the schemes increases almost linearly with the time. However, the slopes, obtained by the linear fitting, are different. The smaller the slope is, the longer time the scheme could simulate to. The SI scheme has the largest slope 1.412×10^{-05} while the OS(2) scheme has the smallest one 2.334×10^{-07} among all the second-order accurate methods. Further, the slopes of the curves of l^∞ errors for the OS(4), P^3-RKDG and P^4-RKDG schemes are almost the same value of 3.199×10^{-13} which is much more smaller than those of the second-order accurate schemes.

Remark 5.1. Both the theoretical and numerical comparison of the OS(2) scheme with the CNO and LCNO schemes show that the former is better, especially in terms of efficiency and error growth. Therefore in some sense this is an answer to the debate stimulated in [53,52] over twenty years ago on which one is most efficient among the OS(2), CNO and LCNO schemes.

Example 5.2. The P^3-RKDG method has been successfully applied before into investigating the interaction for the NLD solitary waves under the quadric scalar self-interaction in [49–51], but the numerical comparison shown in Example 5.1 tells us that the proposed OS(4) scheme should be preferred now. In this example, we further conduct numerical comparison among the OS(4), P^3-RKDG and P^4-RKDG methods in simulating one-humped and two-humped solitary waves. Two typical profiles of the charge density for the NLD solitary wave displayed in Fig. 2 are considered, one denoted by Case 1 has a two-humped profile under the quadric scalar self-interaction, and the other denoted by Case 2 has a one-humped profile under the cubic scalar and vector self-interaction. These two solitary waves are located initially at $x_0 = 5$, travel from right to left with the velocity $V = -0.2$ and stop at the final time $t = 50$. For convenience, we use $\rho_Q(x, t) \equiv J_0$ to represent the charge density.

Table 1
Example 5.1. Part I: Numerical comparison of the accuracy, the conservativeness and the efficiency at $t = 50$ with the time stepsize being set to $\tau = \frac{1}{2}h$. The CPU time in seconds is recorded for the finest mesh.

	h	$\mathcal{V}_Q$	$\mathcal{V}_E$	$\mathcal{V}_P$	err_2	Order	err_∞	Order	Time(s)
CN	0.08	1.38E−15	1.09E−15	2.65E−06	2.74E−02		2.61E−02		
	0.04	4.66E−15	1.37E−15	1.65E−07	6.84E−03	2.00	6.50E−03	2.00	
	0.02	4.78E−15	1.37E−15	1.03E−08	1.71E−03	2.00	1.63E−03	2.00	
	0.01	3.05E−14	2.05E−15	6.42E−10	4.27E−04	2.00	4.06E−04	2.00	367.1
CNO	0.08	7.05E−15	3.24E−08	2.37E−06	2.31E−02		2.21E−02		
	0.04	1.01E−15	2.02E−09	1.47E−07	5.76E−03	2.00	5.51E−03	2.00	
	0.02	5.54E−15	1.26E−10	9.17E−09	1.44E−03	2.00	1.38E−03	2.00	
	0.01	2.88E−14	7.88E−12	5.72E−10	3.59E−04	2.00	3.44E−04	2.00	345.3
LCNO	0.08	2.14E−15	1.83E−06	4.31E−05	2.75E−02		2.62E−02		
	0.04	1.26E−16	2.29E−07	5.55E−06	6.87E−03	2.00	6.53E−03	2.00	
	0.02	8.81E−15	2.86E−08	7.04E−07	1.72E−03	2.00	1.63E−03	2.00	
	0.01	3.11E−14	3.58E−09	8.87E−08	4.29E−04	2.00	4.08E−04	2.00	81.8
LCN1	0.08	2.22E−04	1.92E−04	3.73E−04	3.53E−02		3.34E−02		
	0.04	2.78E−05	2.40E−05	4.65E−05	9.06E−03	1.96	8.56E−03	1.97	
	0.02	3.47E−06	3.01E−06	5.80E−06	2.30E−03	1.98	2.17E−03	1.98	
	0.01	4.34E−07	3.76E−07	7.25E−07	5.78E−04	1.99	5.45E−04	1.99	118.7
LCN2	0.08	2.77E−15	1.64E−07	7.01E−06	2.77E−02		2.64E−02		
	0.04	7.55E−16	1.98E−08	6.77E−07	6.92E−03	2.00	6.58E−03	2.00	
	0.02	7.55E−16	2.44E−09	7.24E−08	1.73E−03	2.00	1.64E−03	2.00	
	0.01	2.91E−14	3.03E−10	8.29E−09	4.32E−04	2.00	4.11E−04	2.00	118.4
HS	0.08	1.62E−06	1.55E−06	4.33E−06	2.00E−02		1.55E−02		
	0.04	1.01E−07	9.65E−08	2.70E−07	5.00E−03	2.00	3.88E−03	2.00	
	0.02	6.30E−09	6.03E−09	1.68E−08	1.25E−03	2.00	9.71E−04	2.00	
	0.01	3.94E−10	3.77E−10	1.05E−09	3.13E−04	2.00	2.43E−04	2.00	14.8
LF	0.08	5.88E−05	4.73E−05	8.68E−06	1.41E−02		1.35E−02		
	0.04	5.51E−06	4.43E−06	6.59E−07	3.51E−03	2.01	3.36E−03	2.01	
	0.02	6.24E−07	5.01E−07	6.91E−08	8.74E−04	2.00	8.36E−04	2.00	
	0.01	7.54E−08	6.05E−08	8.19E−09	2.18E−04	2.00	2.09E−04	2.00	8.9
SI	0.08	3.79E−08	1.15E−07	3.94E−06	3.59E−02		4.76E−02		
	0.04	3.68E−09	8.36E−09	2.40E−07	8.97E−03	2.00	1.19E−02	2.00	
	0.02	4.09E−10	6.87E−10	1.44E−08	2.24E−03	2.00	2.98E−03	2.00	
	0.01	4.89E−11	6.46E−11	8.20E−10	5.60E−04	2.00	7.44E−04	2.00	132.7

Table 2
Example 5.1. Part II: Numerical comparison of the accuracy, the conservativeness and the efficiency at $t = 50$. The CPU time measured in seconds is listed for the finest mesh.

	τ	h	$\mathcal{V}_Q$	$\mathcal{V}_E$	$\mathcal{V}_P$	err_2	Order	err_∞	Order	Time(s)
OS(2)	0.04	0.78	1.04E−13	2.33E−07	3.97E−05	2.03E−03		9.96E−04		
	0.02	0.39	1.33E−13	1.45E−08	2.55E−13	2.53E−04	3.01	1.90E−04	2.39	
	0.01	0.39	3.58E−13	9.04E−10	6.08E−13	6.33E−05	2.00	4.75E−05	2.00	
	0.005	0.20	6.15E−13	5.60E−11	7.13E−13	1.58E−05	2.00	1.21E−05	1.97	8.2
OS(4)	0.04	0.78	7.40E−13	5.78E−13	4.12E−05	1.71E−03		4.27E−04		
	0.02	0.39	1.46E−12	1.25E−12	2.17E−12	7.92E−08	14.40	3.32E−08	13.65	
	0.01	0.20	1.88E−12	1.60E−12	2.71E−12	4.28E−10	7.53	3.28E−10	6.66	
	0.005	0.10	7.00E−13	6.55E−13	2.44E−12	1.93E−11	4.47	1.44E−11	4.51	16.8
P^3−RKDG	0.04	0.78	1.03E−05	5.47E−07	2.61E−06	1.46E−04		1.44E−04		
	0.02	0.39	8.60E−08	5.96E−07	6.31E−07	6.59E−06	4.47	8.85E−06	4.03	
	0.01	0.20	6.98E−10	4.32E−08	4.69E−08	4.10E−07	4.01	5.62E−07	3.98	
	0.005	0.10	7.88E−12	2.75E−09	3.00E−09	2.56E−08	4.00	3.69E−08	3.93	551.6
P^4−RKDG	0.04	0.78	1.00E−07	2.13E−07	1.10E−07	8.02E−06		1.04E−05		
	0.02	0.39	8.53E−10	4.51E−09	3.44E−09	2.58E−07	4.96	3.36E−07	4.96	
	0.01	0.20	2.28E−11	6.41E−11	5.22E−11	8.46E−09	4.93	1.16E−08	4.86	
	0.005	0.10	2.58E−12	9.56E−11	2.16E−10	3.09E−10	4.78	2.39E−10	5.60	744.8

The numerical comparison is shown in Table 3, from which we can observe that, (1) with the same mesh, no matter sparse ($\tau = 0.01$ and $h = \frac{100}{512} \approx 0.1953$) or fine ($\tau = 0.005$ and $h = \frac{100}{1024} \approx 0.0977$), the OS(4) scheme is more conservative and higher accurate than both P^3-RKDG and P^4-RKDG methods; (2) the OS(4) scheme runs much faster than both P^3-RKDG and P^4-RKDG methods as we have found in Table 2. Here, the ratio of the CPU time used by the OS(4) scheme over that used by the P^3-RKDG method is around 5.32%, and reduces to around 4.05% over that used by the P^4-RKDG method for both cases.

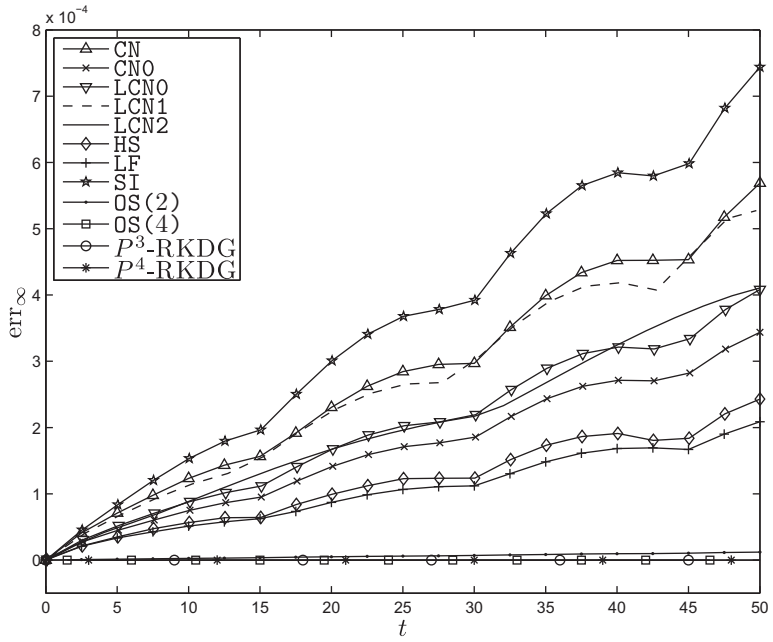

Fig. 1. Example 5.1. The l^∞ error history.

The l^∞ error history is plotted in Fig. 3, which shows that those three methods all have almost zero slope (under 4.50E-09). This can be used to explain our previous success of the P^3-RKDG method in [49–51]. Further more, the more smaller errors of the `OS(4)` method mean that it should be more powerful than others.

It has been shown that the `OS(4)` scheme behaves best for both one-humped and two-humped NLD solitary waves in long time simulations. Therefore, we conclude the comparison with the judgement that the `OS(4)` scheme is the most suitable for simulating the interaction dynamics for the NLD solitary waves in terms of the accuracy, the conservativeness, the efficiency and the error growth. The `OS(4)` scheme will be utilized to investigate the binary collision of the NLD solitary waves. The initial setup is the linear superposition of two moving waves

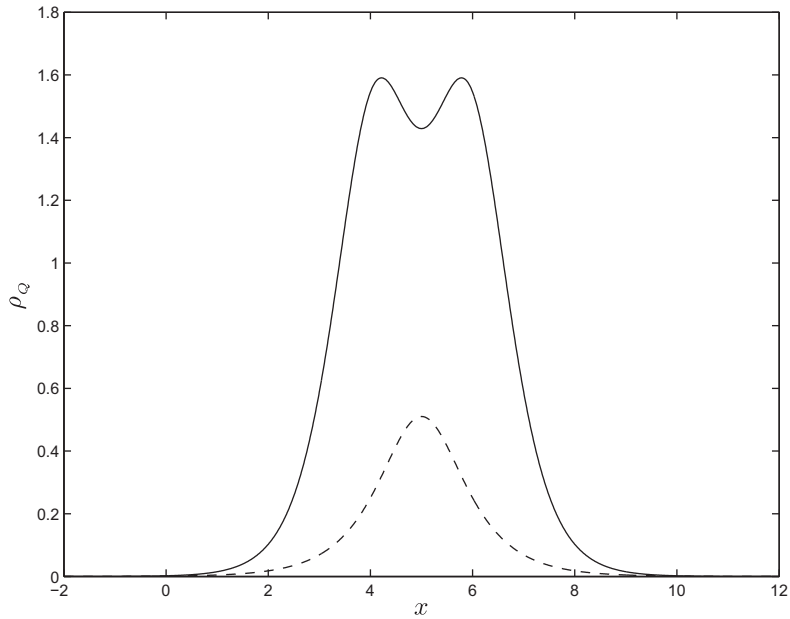

Fig. 2. Example 5.2. The initial charge density $\rho_Q(x,t)$ for two typical cases, $V=-0.2, x_0=5$. Case 1 is shown in the solid line, a two-humped profile ($\omega=0.3$) under the quadric scalar self-interaction ($k=1, s=0.5$ and $v=0$); Case 2 is shown in the dashed line, a one-humped profile ($\omega=0.75$) under the cubic scalar and vector self-interaction ($k=2$ and $s=v=0.5$).

Table 3
Example 5.2. Numerical comparison among the OS(4), P^3-RKDG and P^4-RKDG methods. The CPU time is measured in seconds.

	$\mathcal{V}_Q$	$\mathcal{V}_E$	$\mathcal{V}_P$	err_2	err_∞	Time(s)
Case 1 in the mesh of $\tau = 0.01$ *and* $h = \frac{100}{512}$						
OS(4)	1.96E−12	1.10E−12	3.45E−12	2.15E−09	2.17E−09	7.8
P^3−RKDG	3.34E−08	2.27E−07	2.96E−07	2.89E−06	4.15E−06	146.6
P^4−RKDG	1.35E−12	9.43E−08	5.34E−08	9.02E−08	6.94E−08	195.5
Case 2 in the mesh of $\tau = 0.005$ *and* $h = \frac{100}{1024}$						
OS(4)	9.82E−13	8.35E−13	2.95E−12	7.33E−11	8.63E−11	46.8
P^3−RKDG	3.21E−10	9.04E−09	1.95E−08	2.00E−07	3.98E−07	881.1
P^4−RKDG	9.10E−13	4.89E−09	1.57E−09	4.68E−09	6.35E−09	1156.5

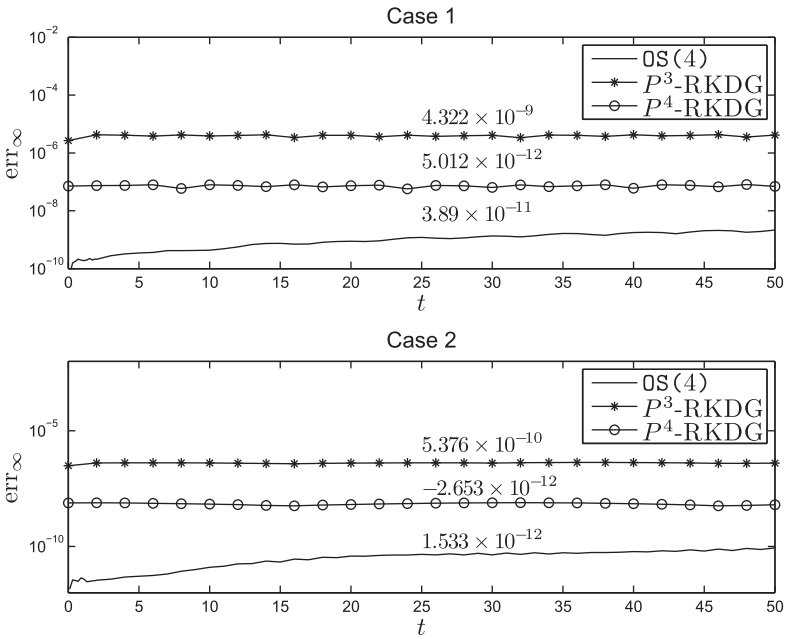

Fig. 3. Example 5.2. The l^∞ error history. The slopes are displayed above the curves.

$$\mathbf{\Psi}(x, t=0) = \mathbf{\Psi}_{\mathrm{l}}^{\mathrm{mw}}(x - x_{\mathrm{l}}, t=0) + \mathbf{\Psi}_{\mathrm{r}}^{\mathrm{mw}}(x - x_{\mathrm{r}}, t=0),$$

where $\mathbf{\Psi}_{pos}^{\mathrm{mw}}(x - x_{pos}, t)$ denote the moving waves (2.23) centered at x_{pos} with the speed V_{pos} and the frequency ω_{pos} for $pos \in \{\mathrm{l}, \mathrm{r}\}$. In the following examples, two equal solitary waves are placed symmetrically at $t = 0$ with $-x_{\mathrm{l}} = x_{\mathrm{r}} = 10$ and $V_{\mathrm{l}} = -V_{\mathrm{r}} = 0.2$. Several typical NLD solitary waves are considered with the parameters given in Table 4, and both quadric ($k = 1$) and cubic ($k = 2$) cases will be studied. It should be noted that the experiments carried out in the literatures are all limited to the collisions of the NLD solitary waves under the quadric scalar self-interaction. A relatively fine mesh, $\tau = 0.005$ and $h = 100/2^{13} \approx 0.0122$, is adopted hereafter.

Table 4
The initial setups of different cases in binary collisions.

case	s	v	$\omega_l = \omega_r$	Remarks
B1	0.5	0	0.8	scalar, one-humped
B2	0	0.5	0.8	vector, one-humped
B3	0.5	0.5	0.8	scalar and vector, one-humped
B4	0.5	0	0.3	scalar, two-humped
B5	4	1	0.1	scalar and vector, two-humped

Example 5.3. The collision of two equal one-humped solitary waves under the scalar self-interaction, *i.e.* Case B1 in Table 4, is studied in this example. The interaction dynamics for the quadric case are shown in the left plot of Fig. 4, where two equal waves with the initial amplitude of 0.4082 move close at a velocity of 0.2 and overlap each other, then separate into a left moving wave and a right moving wave with the amplitude of 0.3743 and the velocity of 0.1831. Similar phenomena are observed for the cubic case shown in the right plot of Fig. 4 except that (1) two waves overlap more stronger around $t = 41$ now due to the stronger nonlinearity; (2) after collision, the amplitude decreases to 0.5899 from the initial amplitude of 0.6455 while the velocity also decreases to 0.1037. In both cases, the discrete charge, energy and linear momentum are approximately conserved in the interaction since the variation of them at $t = 80$ is under 1.58E−10.

Example 5.4. The collision of two equal one-humped solitary waves under the vector self-interaction, *i.e.* Case B2 in Table 4, is studied in this example. To the best of our knowledge, it is the first time to study binary collision of the NLD solitary waves under the vector self-interaction. The interaction dynamics for the quadric case are shown in the left plot of Fig. 5, where the waves keep the shape and the velocity after the collision. A totally different phenomenon appears for the cubic vector self-interaction as displayed in the right plot of Fig. 5. The initial one-humped equal waves first merge into a single wave, then separate and overlap again. Around $t = 50$, collapse happens and highly oscillatory waves are generated and moving outside with a big velocity near 1, meanwhile a one-humped wave with small amplitude is formed at the center. In both cases, the discrete charge, energy and linear momentum are approximately conserved in the interaction since the variation of them at $t = 100$ is under 5.41E−11. Note in passing that the collapse here is different from that shown in [49]. It was reported there that the strong negative energy and radiation appear when the collapse happens during the binary collision of two-humped waves.

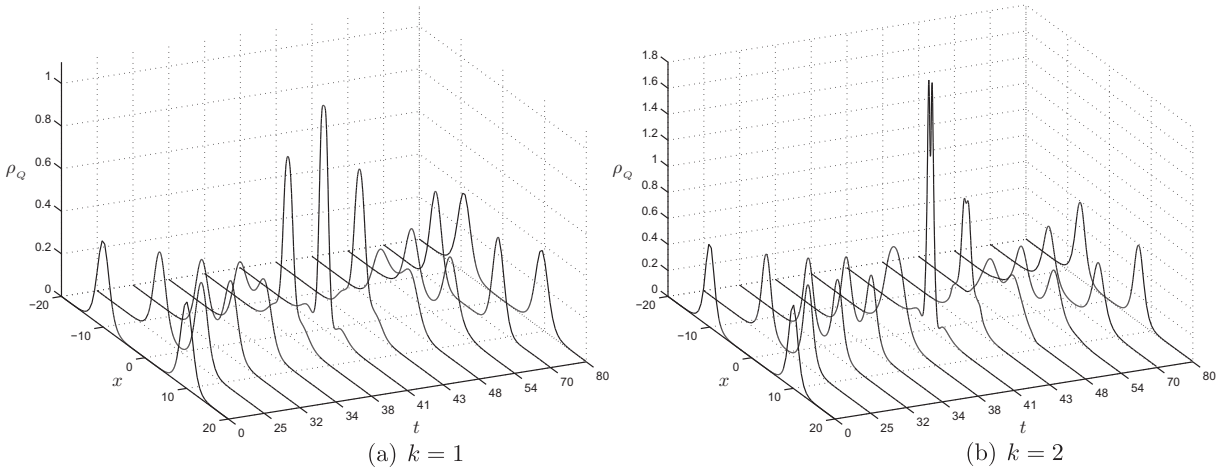

Fig. 4. Example 5.3. Binary collision of the NLD solitary waves under the scalar self-interaction.

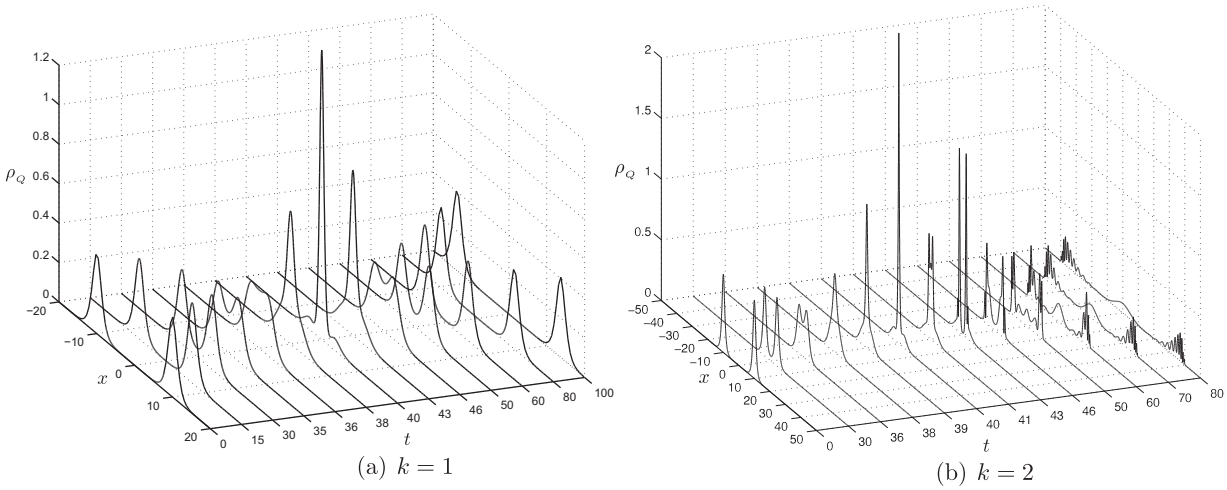

Fig. 5. Example 5.4: Binary collision of the NLD solitary waves under the vector self-interaction.

Example 5.5. This example is devoted into investigating for the first time the collision of two equal NLD solitary waves under the scalar and vector self-interaction, *i.e.* Case B3 in Table 4. The interaction dynamics for the quadric case are shown in the left plot of Fig. 6, where two equal waves with the initial amplitude of 0.2041 move close at a velocity of 0.2 and overlap each other, then separate into a left moving wave and a right moving wave with the amplitude of 0.2091 and the velocity of 0.1968. The collapse similar to that shown in right plot of Fig. 5 happens again for the cubic vector self-interaction, see the right plot of Fig. 6. The initial one-humped equal waves first merge into a single wave at $t = 38$, then separate and overlap again. Around $t = 50$, collapse happens and highly oscillatory waves are generated and moving outside with a big velocity near 1. In both cases, the discrete charge, energy and linear momentum are approximately conserved in the interaction since the variation of them at $t = 80$ is under 3.53E-10.

Example 5.6. As reported before in [49,51], collapse happens in binary and ternary collisions of the NLD solitary waves under the quadric scalar self-interaction if the two-humped waves are evolved. In this example, we will show further that collapse could happen in binary collision of equal two-humped waves under the cubic scalar self-interaction and under the linear combination of scalar and vector self-interactions. First, Case B4 in Table 4 is studied and the interaction dynamics are shown in Fig. 7, which clearly shows that (1) collapse happens in both quadric and cubic cases but is more stronger in the latter; (2) two initial waves at the same velocity are decomposed into groups with different velocities after the collision, but

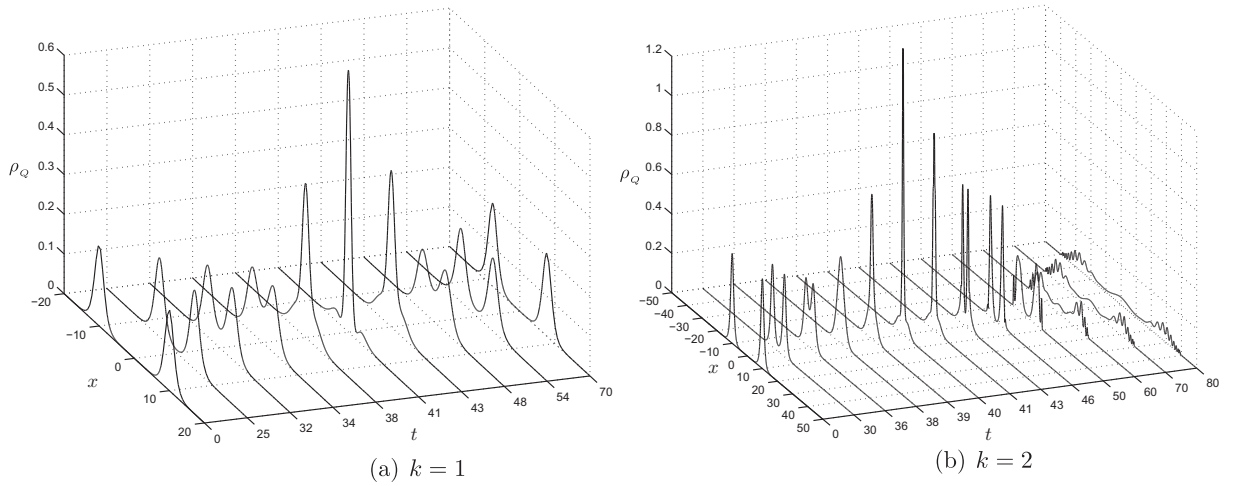

Fig. 6. Example 5.5: Binary collision of the NLD solitary waves under the scalar and vector self-interaction.

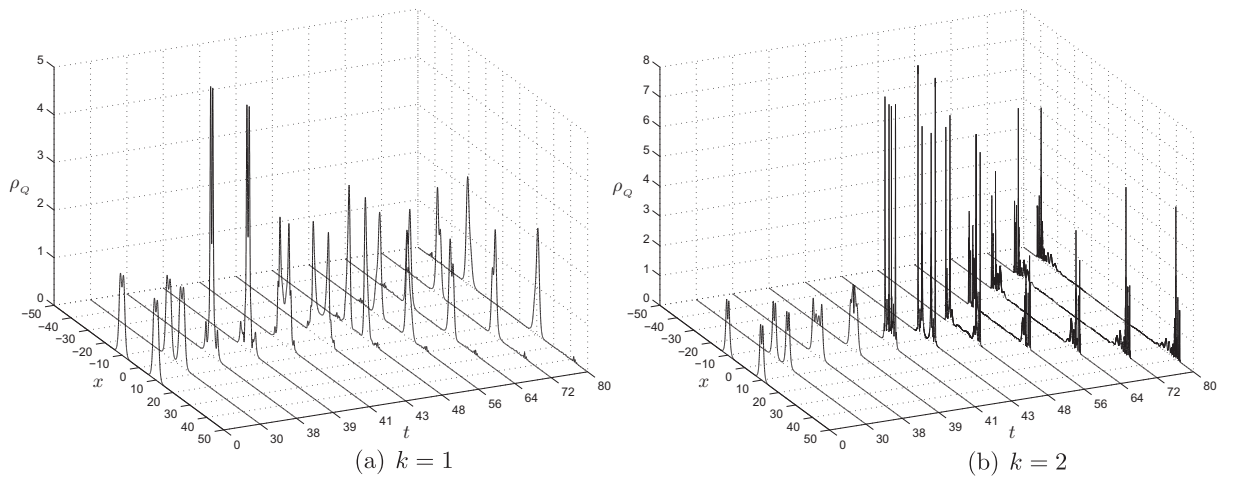

Fig. 7. Example 5.6: Binary collision of the two-humped NLD solitary waves under the scalar self-interaction.

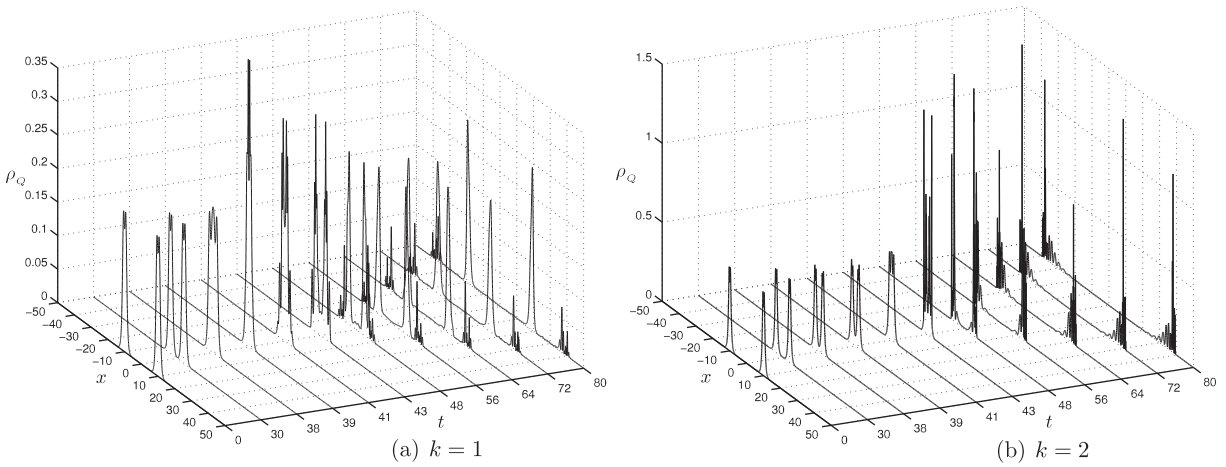

Fig. 8. Example 5.6: Binary collision of the two-humped NLD solitary waves under the scalar and vector self-interaction.

there is no such decomposition for the cubic case. In the left plot of Fig. 7, the highly oscillating waves with small amplitude move outside at a big velocity of 0.9644, while the one-humped waves with big amplitude follow them at a small velocity of 0.4626. In both cases, the discrete charge, energy and linear momentum are approximately conserved in the interaction since the variation of them at $t = 80$ is under 1.01E−5. Second, binary collision of equal two-humped solitary waves under the scalar and vector self-interaction, *i.e.* Case B5 in Table 4, is plotted in Fig. 8. The phenomena are very similar to that shown in Fig. 7, and the "decomposition" phenomenon for the quadric case is more obvious than that shown in the left plot of Fig. 7.

6. Conclusion and outlook

Several numerical methods for solving the NLD equation with the scalar and vector self-interaction have been presented and compared theoretically and numerically. Our results have revealed that among them, the `OS(4)` scheme, one of the fourth-order accurate OS methods, performs best in terms of the accuracy and the efficiency. Particularly, the `OS(4)` scheme is usually more accurate than the P^4-RKDG method in the mesh of the same size, but the former needs much more less computational cost than the latter. Such superior performance of the OS methods is credited to the full use of the local conservation laws of the NLD equation such that the nonlinear subproblems resulted from them are exactly solved. The interaction dynamics for the NLD solitary waves under the quadric and cubic self-interaction have been investigated with the `OS(4)` scheme. We have found that such interaction dynamics depend on the exponent power of the self-interaction. Actually, it has been observed for the first time in our numerical experiments that, (1) collapse happens in collision of two equal one-humped NLD solitary waves under the cubic vector self-interaction but such collapse does not appear for corresponding quadric case; (2) two initial waves at the same velocity are decomposed into groups with different velocities after collapse in binary collision of two-humped NLD solitary waves under the quadric scalar self-interaction or under the quadric scalar and vector self-interaction but such phenomenon does not show up for corresponding cubic case. More efforts on the interaction dynamics for the NLD solitary waves under more general self-interaction with the `OS(4)` method are still going on.

Acknowledgments

Sihong Shao was partially supported by the National Natural Science Foundation of China (Project No. 11101011) and the Specialized Research Fund for the Doctoral Program of Higher Education (Project No. 20110001120112). Huazhong Tang was partially supported by the National Natural Science Foundation of China (Project No. 10925101). The authors would also like to thank the referees for many useful suggestions.

References

[1] P.A.M. Dirac, The quantum theory of the electron, Proc. R. Soc. London A 117 (1928) 610–624.
[2] D.D. Ivanenko, Notes to the theory of interaction via particles, Zhurn. Exp. Teoret. Fiz. 8 (1938) 260–266.
[3] R. Finkelstein, R. Lelevier, M. Ruderman, Nonlinear spinor fields, Phys. Rev. 83 (1951) 326–332.
[4] R. Finkelstein, C. Fronsdal, P. Kaus, Nonlinear spinor field, Phys. Rev. 103 (1956) 1571–1579.
[5] W. Heisenberg, Quantum theory of fields and elementary particles, Rev. Mod. Phys. 29 (1957) 269–278.
[6] A.F. Rañada, Classical nonlinear Dirac field models of extended particles, in: A.O. Barut (Ed.), Quantum Theory, Groups, Fields and Particles, Springer, New York, 1983, pp. 271–291.
[7] H. Weyl, A remark on the coupling of gravitation and electron, Phys. Rev. 77 (1950) 699–701.
[8] W.E. Thirring, A soluble relativistic field theory, Ann. Phys. 3 (1958) 91–112.

[9] M. Soler, Classical, stable, nonlinear spinor field with positive rest energy, Phys. Rev. D 1 (1970) 2766–2769.
[10] D.J. Gross, A. Neveu, Dynamical symmetry breaking in asymptotically free field theories, Phys. Rev. D 10 (1974) 3235–3253.
[11] P. Mathieu, R. Saly, Baglike solutions of a Dirac equation with fractional nonlinearity, Phys. Rev. D 29 (1984) 2879–2883.
[12] S.Y. Lee, T.K. Kuo, A. Gavrielides, Exact localized solutions of two-dimensional field theories of massive fermions with Fermi interactions, Phys. Rev. D 12 (1975) 2249–2253.
[13] S.J. Chang, S.D. Ellis, B.W. Lee, Chiral confinement: an exact solution of the massive Thirring model, Phys. Rev. D 11 (1975) 3572–3582.
[14] P. Mathieu, Compact solitons, bags, and radial excitations, Phys. Rev. D 32 (1985) 3288–3293.
[15] J. Stubbe, Exact localized solutions of a family of two-dimensional nonlinear spinor fields, J. Math. Phys. 27 (1986) 2561–2567.
[16] F. Cooper, A. Khare, B. Mihaila, A. Saxena, Solitary waves in the nonlinear Dirac equation with arbitrary nonlinearity, Phys. Rev. E 82 (2010) 036604.
[17] P. Mathieu, Soliton solutions for Dirac equations with homogeneous non-linearity in (1+1) dimensions, J. Phys. A: Math. Gen. 18 (1985) L1061–L1066.
[18] J. Werle, Non-linear spinor equations with localized solutions, Lett. Math. Phys. 2 (1977) 109–114.
[19] L. Vazquez, Localised solutions of a non-linear spinor field, J. Phys. A: Math. Gen. 10 (1977) 1361–1368.
[20] J. Werle, Stability of particle-like solutions of nonlinear Klein-Gordon and Dirac equations, Acta Phys. Pol. B 12 (1981) 601–614.
[21] P. Mathieu, T.F. Morris, Existence conditions for spinor solitons, Phys. Rev. D 30 (1984) 1835–1836.
[22] T. Cazenave, L. Vázquez, Existence of localized solutions for a classical nonlinear Dirac field, Commun. Math. Phys. 105 (1986) 35–47.
[23] F. Merle, Existence of stationary states for nonlinear Dirac equations, J. Differ. Equ. 74 (1988) 50–68.
[24] M. Balabane, T. Cazenave, A. Douady, F. Merle, Existence of excited states for a nonlinear Dirac field, Commun. Math. Phys. 119 (1988) 153–176.
[25] M. Balabane, T. Cazenave, L. Vázquez, Existence of standing waves for Dirac fields with singular nonlinearities, Commun. Math. Phys. 133 (1990) 53–74.
[26] M.J. Esteban, E. Séré, Stationary states of the nonlinear Dirac equation: A variational approach, Commun. Math. Phys. 171 (1995) 323–350.
[27] M.J. Esteban, E. Séré, An overview on linear and nonlinear Dirac equations, Discrete Cont. Dyn. Syst. 8 (2002) 381–397.
[28] J. Rafelski, Soliton solutions of a selfinteracting Dirac field in three space dimensions, Phys. Lett. B 66 (1977) 262–266.
[29] K. Takahashi, Soliton solutions of nonlinear Dirac equations, J. Math. Phys. 20 (1979) 1232–1238.
[30] A. Alvarez, Spinorial solitary wave dynamics of a (1+3)-dimensional model, Phys. Rev. D 31 (1985) 2701–2703.
[31] P. Kaus, Comment on relation of two-dimensional to asymptotic four-dimensional solitons, Phys. Rev. D 14 (1976) 1722–1724.
[32] W.A. Strauss, L. Vázquez, Stability under dilations of nonlinear spinor field, Phys. Rev. D 34 (1986) 641–643.
[33] A. Alvarez, M. Soler, Stability of the minimum solitary wave of a nonlinear spinorial model, Phys. Rev. D 34 (1986) 644–645.
[34] P. Blanchard, J. Stubbe, L. Vázquez, Stability of nonlinear spinor fields with application to the Gross–Neveu model, Phys. Rev. D 36 (1987) 2422–2428.
[35] I.L. Bogolubsky, On spinor soliton stability, Phys. Lett. A 73 (1979) 87–90.
[36] A. Alvarez, M. Soler, Energetic stability criterion for a nonlinear spinorial model, Phys. Rev. Lett. 50 (1983) 1230–1233.
[37] P. Mathieu, T.F. Morris, Instability of stationary states for nonlinear spinor models with quartic self-interaction, Phys. Lett. B 126 (1983) 74–76.
[38] I.V. Barashenkov, D.E. Pelinovsky, E.V. Zemlyanaya, Vibrations and oscillatory instabilities of gap solitons, Phys. Rev. Lett. 80 (1998) 5117–5120.
[39] M. Chugunova, D. Pelinovsky, Block-diagonalization of the symmetric first-order coupled-mode system, SIAM J. Appl. Dyn. Syst. 5 (2006) 66–83.
[40] D.E. Pelinovsky, A. Stefanov, Asymptotic stability of small gap solitons in the nonlinear Dirac equations,preprint arXiv:1008.4514v1.
[41] L.H. Haddad, L.D. Carr, Relativistic linear stability equations for the nonlinear Dirac equation in Bose–Einstein condensates, EPL 94 (2011) 56002.
[42] A. Comech, On the meaning of the Vakhitov–Kolokolov stability criterion for the nonlinear Dirac equation, arXiv:1107.1763v2.
[43] N. Boussaid, S. Cuccagna, On stability of standing waves of nonlinear Dirac equations, arXiv:1103.4452v3.
[44] G. Berkolaiko, A. Comech, On spectral stability of solitary waves of nonlinear Dirac equation in 1D, Math. Model. Nat. Phenom. 7 (2012) 13–31.
[45] D. Pelinovsky, Survey on global existence in the nonlinear Dirac equations in one dimension, arXiv:1011.5925v1.
[46] N. Bournaveas, G.E. Zouraris, Theory and numerical approximations for a nonlinear 1+1 Dirac system, ESAIM: M2AN 46 (2012) 841–874.
[47] A. Alvarez, B. Carreras, Interaction dynamics for the solitary waves of a nonlinear Dirac model, Phys. Lett. A 86 (1981) 327–332.
[48] A. Alvarez, P.Y. Kuo, L. Vázquez, The numerical study of a nonlinear one-dimensional Dirac equation, Appl. Math. Comput. 13 (1983) 1–15.
[49] S.H. Shao, H.Z. Tang, Interaction for the solitary waves of a nonlinear Dirac model, Phys. Lett. A 345 (2005) 119–128.
[50] S.H. Shao, H.Z. Tang, Higher-order accurate Runge–Kutta discontinuous Galerkin methods for a nonlinear Dirac model, Discrete Cont. Dyn. Syst. B 6 (2006) 623–640.
[51] S.H. Shao, H.Z. Tang, Interaction of solitary waves with a phase shift in a nonlinear Dirac model, Commun. Comput. Phys. 3 (2008) 950–967.
[52] J. De Frutos, J.M. Sanz-Serna, Split-step spectral schemes for nonlinear Dirac systems, J. Comput. Phys. 83 (1989) 407–423.
[53] A. Alvarez, Linearized Crank–Nicholson scheme for nonlinear Dirac equations, J. Comput. Phys. 99 (1992) 348–350.
[54] S. Jiménez, Derivation of the discrete conservation laws for a family of finite difference schemes, Appl. Math. Comput. 64 (1994) 13–45.
[55] Z.Q. Wang, B.Y. Guo, Modified Legendre rational spectral method for the whole line, J. Comput. Math. 22 (2004) 457–474.
[56] J.L. Hong, C. Li, Multi-symplectic Runge–Kutta methods for nonlinear Dirac equations, J. Comput. Phys. 211 (2006) 448–472.
[57] H. Wang, H.Z. Tang, An efficient adaptive mesh redistribution method for a nonlinear Dirac equation, J. Comput. Phys. 222 (2007) 176–193.
[58] L.H. Haddad, L.D. Carr, The nonlinear Dirac equation in Bose–Einstein condensates: foundation and symmetries, Physica D 238 (2009) 1413–1421.
[59] B. Saha, Nonlinear spinor fields and its role in cosmology, Int. J. Theor. Phys. 51 (2012) 1812–1837.
[60] S. Coleman, Quantum sine-Gordon equation as the massive Thirring model, Phys. Rev. D 11 (1975) 2088–2097.
[61] Y. Nogami, F.M. Toyama, Transparent potential for the one-dimensional Dirac equation, Phys. Rev. A 45 (1992) 5258–5261.
[62] Q.S. Chang, E.H. Jia, W. Sun, Difference schemes for solving the generalized nonlinear Schrödinger equation, J. Comput. Phys. 148 (1999) 397–415.
[63] P. Gordon, Nonsymmetric difference equations, SIAM J. Appl. Math. 13 (1965) 667–673.
[64] Q. Sheng, Solving linear partial differential equations by exponential splitting, IMA J. Numer. Anal. 9 (1989) 199–212.
[65] S.A. Chin, Structure of positive decompositions of exponential operators, Phys. Rev. E 71 (2005) 016703.
[66] A.T. Sornborger, E.D. Stewart, Higher-order methods for simulations on quantum computers, Phys. Rev. A 60 (1999) 1956–1965.
[67] M. Thalhammer, M. Caliari, C. Neuhauser, High-order time-splitting Hermite and Fourier spectral methods, J. Comput. Phys. 228 (2009) 822–832.
[68] C.W. Shu, High order weighted essentially nonoscillatory schemes for convection dominated problems, SIAM Rev. 51 (2009) 82–126.